JACS
JOURNAL OF THE AMERICAN CHEMICAL SOCIETY

ARTICLE

pubs.acs.org/JACS

Molecular Optimization of Multiply-Functionalized Mesoporous Films with Ion Conduction Properties

George L. Athens,[†] Donghun Kim,[†] Jan D. Epping,[†,‡] Sylvian Cadars,[†,§] Yair Ein-Eli,[∥] and Bradley F. Chmelka*[,†]

[†]Department of Chemical Engineering, University of California, Santa Barbara, California 93106, United States
[∥]Department of Materials Engineering, Technion—Israel Institute of Technology, 32000 Haifa, Israel

Supporting Information

ABSTRACT: Sequential processing of multiply functionalized mesoporous films is shown to yield materials that are compositionally and structurally heterogeneous on mesoscopic and molecular length scales, both of which must be controlled to optimize macroscopic ion-conduction properties. Cubic mesoporous silica films prepared from strongly *acidic* solutions were subsequently functionalized under highly *alkaline* conditions to incorporate hydrophilic aluminosilica surface moieties, followed by *nonaqueous* conditions to introduce perfluorosulfonic-acid surface groups. Such sequential combination of individually incompatible steps yielded stable mesoporous films with high surface hydrophilicities and strong acid functionalities that exhibited high proton conductivities (ca. 9×10^{-2} S/cm) at elevated temperatures (120 °C). Molecular, mesoscopic, and macroscopic properties of the multiply functionalized films were monitored and correlated at each stage of the syntheses by nuclear magnetic resonance (NMR) spectroscopy, small-angle X-ray scattering (SAXS), transmission electron microscopy (TEM), elemental analysis, adsorption, and ion conductivity measurements. In particular, variable-temperature solid-state two-dimensional (2D) ^{27}Al{^{1}H}, ^{29}Si{^{1}H}, ^{27}Al{^{19}F}, and ^{29}Si{^{19}F} HETeronuclear chemical-shift CORrelation (HETCOR) NMR spectra reveal separate surface adsorption and grafting sites for the different functional surface species within the mesopore channels. The hydrophilic aluminosilica and acidic fluoro-group loadings and interaction sites are demonstrated to be strongly affected by the different synthesis and functionalization treatments, which must be separately and collectively optimized to maximize the proton conductivities.

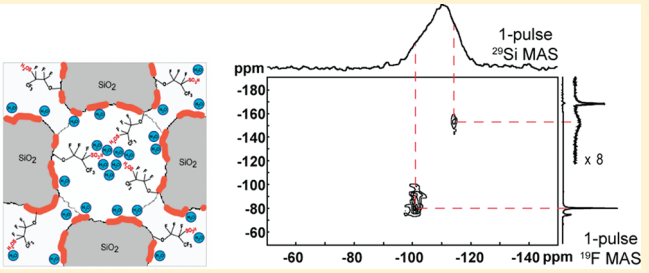

INTRODUCTION

Functionalization of porous inorganic solids can be used to produce materials with novel properties that derive from their heterogeneous structures and diverse compositions. Different functionalities can be combined to introduce properties that are additive or have synergistic local effects. In heterogeneous catalysis, this has a long history, as exploited for example in metal/acid,[1,2] bimetallic,[3−6] or more recently tandem catalyst systems,[7,8] which typically have been in the form of powders, for example, zeolite molecular sieves,[9] amorphous or crystalline metal oxides,[10,11] or mesoporous solids.[12−16] Recently, processing opportunities presented by block-copolymer-directed mesostructured solids have led to materials in film, fiber, and monolith morphologies that have been functionalized with multiple species to obtain different property combinations.[17−22] In many syntheses, emphases have been placed on so-called 'one-pot' protocols in which multiple components, including functional species, are incorporated simultaneously during self-assembly and formation of the inorganic network.[23−27] These, however, rely on the collective compatibilities of the various components under the synthesis conditions used, which often limits the extent and diversity of the functionalities that can be introduced.

Organic functionalization of mesoporous inorganic materials in particular has generated considerable attention,[23,28,29] due to the attractiveness of combining a wide range of organic compound properties with the robust thermal and mechanical stabilities of high-surface-area inorganic solids. The anchoring of organic moieties to mesoporous inorganic surfaces by covalent bonds has generally followed two protocols, either by co-condensation of the functional species as the inorganic framework cross-links[23−27,30−33] or by postsynthetic grafting of the species to accessible pore surfaces after the framework has been formed.[23−27,34−36] Siliceous frameworks have been frequently prepared, due to the versatility of silica sol−gel chemistry, the compatibility of soluble precursors with block-copolymer self-assembly agents, and the suitability of condensed networks for postsynthesis grafting or modification. In the case of silica, co-condensation involves the simultaneous cross-linking of hydrolyzed

Received: April 26, 2011
Published: September 16, 2011

tetraalkoxysilanes ($(RO)_4Si$) with hydrolyzed trialkoxyorganosilanes ($(RO)_3SiR'$, where R and R′ are organic moieties), which in the presence of a structure-directing surfactant agent yields mesostructured organically modified silica.[14,30,37−39] While co-condensation leads to the incorporation of the functional species in a single process step, removal of the surfactant species is usually required to produce the porosity needed to allow access to the functional sites in the mesopore channels. High concentrations of the precursor species tend to disrupt mesostructural ordering[23] and make it difficult to control particle or other bulk (e.g., film, fiber, or monolith) morphologies. Additional challenges arise as the synthesis mixtures become more complicated, for example, when additional co-solvent or functional species are present, due to often competing or incompatible conditions required for their coassembly.

In contrast, postsynthesis grafting methods are based primarily on the reactions of organosilanes ($(RO)_3SiR'$) or halosilanes (e.g., Cl_3SiR') with silanol groups on the interior mesopore channels of previously prepared (e.g., self-assembled and then calcined or solvent-extracted) mesoporous silica.[40−43] This functionalization approach allows for a wide range of organic species to be anchored to silica surfaces without significantly affecting the mesostructural ordering of the silica support. If appropriate silane species are not available, then alternative surface-anchoring chemistries can be used, provided suitable grafting moieties and conditions can be found. In addition, controlling the density and distributions of grafted species is generally challenging. Nevertheless, the versatile processability of mesostructured block-copolymer-directed silica permits facile control over particle, film, fiber, or monolith morphologies and separate incorporation and optimization of multiple functional species, as will be shown below.

Cubic mesostructured aluminosilica with strong acid moieties represents a technologically important example of multiply functionalized inorganic materials that, as films, yield attractive proton-conduction properties at elevated temperatures.[44] Among the challenges to preparing such materials are the incompatibilities of the synthesis conditions required to incorporate the different individual functional components into the mesostructured films. Block-copolymer-directed silica mesophases can be formed from strongly *acidic* solutions, which allow highly ordered cubic mesostructured silica films to be synthesized. After calcination to remove the block-copolymer species, hydrophilic aluminosilica surface moieties can be introduced to the interior mesopore channels under highly *alkaline* solution conditions, followed by separate covalent grafting of perfluorinated-sulfonic-acid (PFSA) groups from *nonaqueous* solvents to introduce ion-conducting properties. This sequential synthesis protocol overcomes several previously severe materials limitations to yield complex materials with robust interconnected channels in films that can sustain proton-conducting properties above 120 °C. Under such conditions, these membranes maintain high proton conductivities that permit operation of hydrogen fuel cells at temperatures where, for example, CO poisoning of the anode catalyst can be mitigated, but membrane dehydration may otherwise be severely limiting.[45]

Crucially, the properties of multiply functionalized mesostructured silica films can be enhanced by understanding and optimizing certain heterogeneities in local material compositions and structures. These include heterogeneities in the types, reactivities, and distributions of surface grafting sites, whose differences allow the introduction, coexistence, and optimization of mixed functionalities that are not generally achievable under a common set of synthesis conditions or have not been demonstrated in polymeric or hybrid membrane materials.[46−48] For example, many wholly polymeric materials rely on hydrated ion-conducting channels that tend to close at low humidities or at elevated temperatures as they dehydrate. The blending of zeolite or mesoporous silica powders into such polymeric materials has led to increased overall hydrophilicity,[49−53] although the stabilities of the ion-conducting channels remain those of the continuous polymer host matrices, which tend still to close at low ambient humidities.[49,53] A recent report of an inorganic−organic membrane material based on anodized and functionalized porous silicon was shown to have promising hydrophilic and proton-conducting properties at low humidity and ambient temperature conditions.[54]

Here, we show how sequenced-processing strategies can be combined with detailed characterization over multiple length scales, especially at a molecular level, to design and optimize complex multifunctional solids with combinations of properties that have been challenging to obtain in ion-conducting materials. A series of discrete synthesis steps under otherwise mutually incompatible conditions, for example, from acidic, alkaline, and/or nonaqueous solutions, allow different functionalities to be introduced and optimized by using molecular-level understanding obtained from powerful two-dimensional (2D) solid-state correlation NMR techniques. Such methods are sensitive to local interactions among different surface moieties and thus yield detailed insights on the proximities and distributions of the different molecular components. Combined with complementary techniques, such as small-angle X-ray diffraction, electron microscopy, elemental analyses, and adsorption and conductivity measurements, the results provide new understanding of coupled and often competitive molecular interactions that can be correlated and controlled to enhance macroscopic proton conductivities and thermal stabilities.

MATERIALS AND METHODS

Material syntheses. Mesostructured block-copolymer/silica films with body-centered-cubic ($Im\bar{3}m$ space group) structures were synthesized according to a procedure that has been described previously.[44,55] Typically, a solution containing 8.2 g of tetraethoxysilane (TEOS) hydrolyzed in 0.007 g of HCl, 3.6 g of water, and 12 g of ethanol was combined with a second solution containing 2.0 g of poly(ethylene oxide)-poly(propylene oxide)-poly(ethylene oxide) triblock copolymer ($EO_{106}PO_{70}EO_{106}$, Pluronic F127, BASF) dissolved in 20 g of ethanol. The resulting mixture was stirred for 2 h at room temperature, subsequently poured into a loosely covered polystyrene Petri dish, and allowed to stand at a controlled temperature of 25 °C for 3−5 days. During this time, the ethanol and water co-solvents evaporated and mesostructural ordering of the triblock copolymer and cross-linking of the silica precursor species occurred to yield free-standing transparent cubic mesostructured block-copolymer/silica films that were 100−220 μm thick. The as-synthesized films were calcined to remove the structure-directing triblock copolymer species by heating at 1 °C/min to 550 °C in air and holding at this temperature for 12 h, which resulted in mesoporous silica films with thicknesses of 80−180 μm.

Incorporation of aluminosilica moieties onto the interior of the initially silica mesopore surfaces was achieved by covalently grafting soluble aluminosilica precursor species in alkaline solution (pH∼11).[56] Two grams of the free-standing mesoporous silica films were placed in a polypropylene bottle containing 100 mL of 0.025 M solution of hydrolyzed $NaAlO_2$ and heated at 60 °C under gentle stirring for

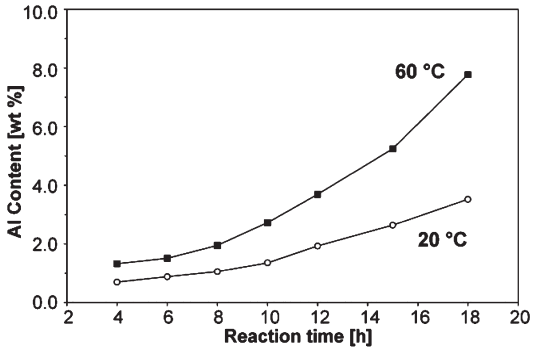

Figure 1. Aluminum contents in aluminosilica-grafted cubic mesoporous silica films as functions of reaction time and temperature in alkaline (pH∼11) aluminate solutions.

12 h. Samples with maximum aluminum content were reacted at 60 °C for 18 h; shorter times led to lower extents of aluminosilica incorporation. The aluminosilica-grafted mesoporous films were repeatedly washed with deionized water, followed by soaking in 1.0 M H_2SO_4 twice to ion-exchange Na^+ for H^+ ions in the films and rinsing in deionized water, until no further changes in pH were observed. Because of the alkaline conditions of the grafting solution, Si−O−Si bonds undergo partial cleavage, thus, promoting inclusion of hydrolyzed aluminum hydroxide species at the otherwise siliceous mesopore surfaces. For example, Figure 1 shows elemental analysis results for cubic mesoporous silica films exposed to the same alkaline (pH∼11) aluminate solution, as functions of reaction time at 20 or 60 °C. At higher temperatures and longer reaction times, higher aluminosilica grafting densities were achieved, up to 7.8 wt % Al after 18 h at 60 °C, without significant deterioration of the cubic mesostructural ordering of the films. Still higher aluminosilica concentrations can be incorporated at longer reaction times (>18 h) and temperatures above 60 °C, though at the expense of mesostructural ordering, which is accompanied by diminished mechanical and structural integrities of the films.

Perfluorosulfonic-acid (PFSA) species were covalently grafted onto the aluminosilica mesopore surfaces under nonaqueous conditions. Two grams of the ion-exchanged, mesoporous aluminosilica films were reacted with 1.0 g of 1,2,2-trifluoro-2-hydroxy-1-trifluoromethylethane-sulfonic-acid-beta-sultone (used as-received from Matrix Scientific, Columbia, SC) in 25 mL of dry (<0.005% H_2O) toluene at 110 °C for 4 h.[40] The perfluorosulfonic-acid-grafted aluminosilica films were subsequently washed with anhydrous toluene and dried at 100 °C in air. Finally, the PFSA-grafted mesoporous aluminosilica films were treated with aqueous triflic acid (CF_3SO_3H) solutions to fill the remaining mesopore volumes with CF_3SO_3H species. Identical films were soaked at room temperature for 1 h in solutions containing different concentrations of triflic acid from 0 to 7.0 M (in 0.5 M increments) CF_3SO_3H (aq) to obtain materials with a range of triflic-acid and water contents to which proton conductivities were correlated. Identical PFSA- and triflic-acid-functionalization procedures were used for the mesoporous silica films that were not grafted first with aluminosilica species.

Characterization. 2D small-angle X-ray scattering (SAXS) patterns and transmission electron microscopy (TEM) images were acquired to establish the degree of mesostructural ordering in the films. SAXS patterns were obtained using 1.54 Å Cu Kα radiation generated by a fine-focus (0.2 mm) Rigaku rotating-angle generator and detected on a Bruker HI-STAR multiwire area detector. The free-standing silica films were positioned in the sample holder in transmission mode. 1D diffraction patterns were obtained from the 2D scattering data by azimuthal integration. TEM samples were prepared by grinding the free-standing films into powders, forming slurries of the powders in ethanol, and dispersing them onto a holey carbon grid. TEM images were collected on a JEOL 2010 microscope operating at 200 kV.

Elemental analyses were performed to quantify the bulk Si/Al molar ratios in the mesoporous aluminosilicas by using a TJA IRIS Inductively Coupled Plasma (ICP) spectrometer. The thermal stabilities and quantities of the various species within the mesopores of the functionalized perfluorosulfonic-acid-grafted aluminosilica films containing triflic acid were evaluated by thermogravimetric analyses (TGA), in combination with mass spectrometry of the effluent gases. The TGA measurements (to ±1 wt %) were made using a Mettler TGA/sDTA851e ThermoGravimetric Analyzer coupled to a Blazers ThermoStar mass spectrometer. The functionalized films were heated from 25 to 600 °C at a rate of 10 °C/min under constant nitrogen gas flow of 50 mL/min.

Solid-state nuclear magnetic resonance (NMR) spectroscopy was used to characterize the local compositional and structural environments of molecular species in the materials, especially those residing along the interior mesopore wall surfaces. NMR measurements were performed on identical functionalized films as those used for the proton conductivity measurements, with the exception that the films were gently ground to produce powders that were amenable for NMR investigation. Solid-state one-dimensional (1D) and two-dimensional (2D) NMR experiments were acquired on a Bruker AVANCE-300 NMR spectrometer, with a wide-bore 7.0 T magnet, operating at 300.08, 282.34, 78.20, and 59.62 MHz, for ^1H, ^{19}F, ^{27}Al, and ^{29}Si, respectively. The measurements were performed under conditions of magic-angle spinning (MAS) using a 4 mm Bruker double-resonance broadband MAS probehead with variable temperature capabilities. Use of a high-frequency splitter box permitted high-power proton decoupling during ^{19}F excitation and detection. 2D HETeronuclear chemical-shift CORrelation (HETCOR) NMR experiments[57,58a] allowed dipole−dipole-coupled nuclei to be identified according to their isotropic chemical shifts in 2D frequency maps. This greatly enhances spectral resolution, thereby enabling nearby (ca. 1 nm) molecular species to be established. Solid-state HETCOR NMR measurements were carried out under MAS conditions at 6 kHz and at low temperature (−30 °C) to reduce influences from molecular mobility, which can reduce dipolar coupling strengths. In particular, temperatures ≤ −30 °C were required for effective cross-polarization between the aluminosilica and otherwise relatively mobile triflic acid species. For the 2D $^{29}Si\{^1H\}$ HETCOR spectra, a 4.8 μs ^1H 90° pulse, followed by a 2 ms contact time, were used for cross-polarization, and 512 signal acquisitions were collected with a 6 s recycle delay for 96 t_1 increments, resulting in a total measurement time of 82 h. For the 2D $^{27}Al\{^1H\}$ HETCOR spectra, a 4.8 μs ^1H 90° pulse, followed by a 1 ms contact time, were used for cross-polarization, and 896 acquisitions were collected with a 2 s recycle delay for 48 t_1 increments (24 h duration). In both the 2D $^{29}Si\{^{19}F\}$ and $^{27}Al\{^{19}F\}$ HETCOR experiments, 5.5 μs ^{19}F 90° pulses were used. For the 2D $^{29}Si\{^{19}F\}$ HETCOR measurements, an 8 ms contact time and a 5 s recycle delay were used, and 5120 acquisitions were collected for 32 t_1 increments (228 h duration). For the 2D $^{27}Al\{^{19}F\}$ HETCOR spectra, 5 ms contact time with a 5 s recycle delay were used, and 2048 acquisitions were collected for 32 t_1 increments (91 h duration). Contact times longer than 5 ms could not be used for the $^{27}Al\{^1H\}$ and $^{27}Al\{^{19}F\}$ HETCOR measurements, due to short ^{27}Al $T_{1\rho}$ relaxation times of several hundred microseconds.[57] Low ^{27}Al radio frequency (B_1) fields of 17 and 15 kHz were used to establish cross-polarization matching conditions during the contact times of the $^{27}Al\{^1H\}$ and $^{27}Al\{^{19}F\}$ HETCOR experiments, respectively. The ^1H and ^{29}Si chemical shifts were referenced to tetramethylsilane (TMS) using tetrakis(trimethylsilyl)silane $[(CH_3)_3Si]_4Si$ as a secondary standard (0.25 ppm for the ^1H signal of the methylsilyl groups and −9.84 and −135.40 ppm for the trimethylsilyl and silane ^{29}Si signals, respectively).[58b] The ^{19}F chemical shifts were referenced to $CFCl_3$ using polytetrafluoroethylene $[(-CF_2-CF_2-)_n]$ as

a secondary standard (−122 ppm), and the ^{27}Al chemical shifts were referenced to an aqueous 0.5 M aluminum nitrate [$Al(NO_3)_3$] solution.[58c]

Quantitative solid-state 1D ^{27}Al MAS spectra were acquired with sample spinning rates of 10 kHz and by applying single 30° ^{27}Al pulses with recycle delays of 7 s. Integration of the resulting ^{27}Al signals allowed their relative quantification. A dense and known mass of aluminum nitride (AlN, 2 mg) was additionally used as an internal ^{27}Al spin-counting standard to establish the absolute populations of different aluminosilica species detected. Quantitative ^{27}Al NMR measurements are challenging, due to the quadrupolar character of $I = 5/2$ ^{27}Al nuclei and interactions between their nuclear quadrupole moments and local electric field gradients. Compared to spin $I = 1/2$ nuclei, such as ^{1}H, ^{19}F, ^{29}Si, and so forth, under similar conditions of conventional MAS, anisotropic interactions of quadrupolar nuclei, such as ^{27}Al, are only partially averaged, leading often to significant centerband broadening from anisotropic second-order quadrupolar effects.[59] Furthermore, because the electric field gradient in the vicinity of a given ^{27}Al nucleus increases with decreasing symmetry of the nearby electronic environment, substantial additional broadening of ^{27}Al signals can result for species in locally distorted sites, such as found in amorphous solids or at solid surfaces. Such spectral broadening may be so severe for quadrupolar nuclei in distorted environments that the signals become broadened into the baseline, resulting in a substantial fraction of the aluminosilica species being unobservable by ^{27}Al MAS NMR (so-called "NMR-invisible" ^{27}Al species).[60] Quantitative solid-state ^{27}Al NMR signals were correlated with bulk elemental analyses to evaluate the fractions of NMR-visible and invisible ^{27}Al species and establish that signals from nearly all ^{27}Al species present were detected in the materials investigated.

Because both aluminosilica- and PFSA-grafted species compete for covalent attachment to surface silanol sites, their relative surface coverages were expressed and normalized relative to the number of surface silanol groups that were present after calcination of the as-synthesized films and before subsequent functionalization treatments. The absolute number of such silanol species was determined from quantitative 1D ^{29}Si MAS NMR spectra (Supporting Information, Figure S1), which yielded signals at −102 and −110 ppm, corresponding to Q^3 silanol moieties and fully condensed Q^4 framework silica species, respectively. The relative integrated intensities of these ^{29}Si MAS signals remained unchanged within ±10% following each of the alkaline, nonaqueous, and acid functionalization treatments.

Bulk proton conductivity in the temperature range 100−140 °C was the principal macroscopic property criterion used to optimize the various functionalization steps. Proton conductivities were measured by AC impedance spectroscopy using a Solartron 1260 Impedance/Gain-Phase Analyzer over the frequency range 0.1 Hz to 1 MHz with an AC amplitude of 10 mV. The ohmic resistances of the films were extracted from Nyquist impedance plots generated using the ZPlot/ZView software package and were converted to conductivities by using the initial dimensions of dried membranes. For the measurements, the films were dried at 50 °C for a day under vacuum and were then placed identically in a Teflon cell using two platinum foils as back-contact electrodes. The proton conductivity of each film was measured as functions of temperature and relative humidity (R.H.). The measurement cell containing a given film was placed in a stainless-steel environmental chamber, along with a known quantity of deionized water that depended upon the amount required to yield the desired relative humidity at each temperature. Each film was allowed to equilibrate (typically ∼1 h) at each temperature and humidity prior to measurement of its proton conductivity.

Modeling. Calculations at the density functional level of theory (DFT) were performed with Gaussian 03,[61] using the B3-LYP[62,63] hybrid functional. Partial geometry optimizations were achieved using standard 6-31G (for H atoms) and 6-31G* (for all other atoms) basis sets. ^{29}Si NMR shielding calculations were carried out using gauge-including atomic orbitals[64] (GIAO), and locally dense basis sets using IGLO-III[65] (as obtained from the EMSL basis-set database[66,67]) for the Si atoms at the grafting site and its first Si nearest neighbors, 6-31++G*, for the other Si atoms and the O, C, and F atoms, and 6-31++G for the H atoms. Because the silica frameworks in the walls of the mesoporous material are highly disordered, the local structures of the grafting sites are not well-defined. DFT calculations of NMR parameters were conducted instead on model surface clusters extracted from an ordered silicate framework structure proposed elsewhere for surfactant-directed layered silicates.[68] Such model clusters contain Q^3 ^{29}Si moieties that represent potential grafting sites in a HO−**Si**[$O_{12}Si_{10}$] fragment, in which the other Si and O atoms were kept in their initial geometries. Hydrogen atoms (12 total) were then added to the nonbridging oxygen atoms and to the second-nearest-neighbor Si atoms, after which the H positions were subsequently relaxed, along with the grafted molecule and the oxygen atom that links it to the Si atom at the grafting site.

RESULTS AND DISCUSSION

Novel acid-functionalized cubic mesoporous aluminosilica films were synthesized via a versatile 'sequential processing' protocol that allows for independent adjustment of the conditions under which the various components are incorporated. Free-standing mesoporous silica films resulted from cooperative self-assembly of $EO_{106}PO_{70}EO_{106}$ triblock-copolymer species and a network-forming inorganic precursor species (hydrolyzed silica) under acidic (pH 1.5) conditions during evaporation of volatile solvents (ethanol and water).[55,69] The structure-directing block-copolymer species were subsequently removed from the mesostructured films by calcination, leaving behind mesoporous silica films. For the synthesis conditions used here, small-angle X-ray scattering results and transmission electron micrographs (Supporting Information, Figure S2) established that the mesoporous silica films were three-dimensionally ordered with a body-centered-cubic ($Im\bar{3}m$) structure and a d_{110} spacing of 11.7 nm. Analyses of nitrogen adsorption isotherms (Supporting Information, Figure S3) revealed that the films had mesopores with mean diameters of 8.5 nm and surface areas of ∼350 m^2/g that could be subsequently functionalized.

Hydrophilic moieties were introduced along the interior mesopore surfaces through postsynthetic grafting of aluminosilica species under alkaline (pH∼11) solution conditions. The presence of aluminosilica surface sites in the mesopores was expected to improve significantly water retention of the materials at elevated temperatures (100−200 °C). The incorporation of co-condensed aluminosilica species during formation of cubic mesostructured films was not possible under the conditions used and resulted in the precipitation of separate silica and alumina particles and poor film ordering. In contrast, superior control over mesostructural framework order, film quality, and mechanical/hydrothermal stabilities was achieved by postsynthetic grafting of hydrophilic aluminosilica species at desirable mesopore surface locations in cubic mesoporous silica films. Further functionalization of the hydrophilic mesopore surfaces by covalent grafting of perfluorosulfonic-acid species under nonaqueous conditions and subsequent pore-filling with aqueous triflic acid (CF_3SO_3H) solutions yielded robust films with stable proton conductivity properties at temperatures well above 100 °C. By understanding and controlling the compositions, structures, and surface interactions of molecular species within the mesoporous films, their macroscopic ion-conduction properties can be enhanced.

Table 1. Elemental Analyses and Solid-State Single-Pulse ^{27}Al MAS NMR Quantification of the Aluminum Contents of Films Following a Sequence of Different Functionalization Treatments for Cubic Mesoporous Silica, Aluminosilica, PFSA-Grafted Aluminosilica, and PFSA-Grafted Aluminosilica Containing 8 wt % CF_3SO_3H[a]

	elemental analysis		1-pulse ^{27}Al MAS NMR	
functionalized cubic mesoporous films	Si/Al molar ratio	wt% Al	Al^{IV} (%)	Al^{VI} (%)
silica	∞	0	-	-
aluminosilica	15.6 ± 0.5	3.7	92	8
PFSA-aluminosilica	16.8 ± 0.4	3.5	39	61
PFSA-aluminosilica with 8 wt % CF_3SO_3H	16.9 ± 0.2	3.5	1	99

[a] All of the films were prepared from the same cubic mesoporous silica film template and exposed to identical aluminosilica- and PFSA-grafting solutions, as appropriate.

Such insights yield key molecular design and processing criteria that allow the incorporation and collective optimization of multiple functional properties, even those that may rely on incompatible synthesis conditions.

Bulk Aluminosilica Composition. The extent of incorporation of hydrophilic aluminosilica moieties onto the interior mesopore surfaces depends on temperature, composition (e.g., pH) of the alkaline grafting solution, and the time the solution is allowed to contact the mesoporous silica films. Bulk aluminosilica concentrations in the mesoporous films were determined by elemental analyses after each step of the 'sequential functionalization' protocol. Table 1 shows bulk Si/Al elemental analysis results for a mesostructured silica film, aluminosilica-grafted film, PFSA-grafted aluminosilica film, and PFSA-grafted aluminosilica film containing 8 wt % triflic acid backfilled into the mesopores. Incorporation of aluminosilica into the silica films for 12 h at 60 °C yielded a material with a Si/Al molar ratio of 15.6 ± 0.5 (3.7 wt % Al). During the subsequent grafting of the perfluorosulfonic-acid species, ~8% of the aluminum atoms in the aluminosilica-grafted silica film were lost to the perfluorosulfonic-acid grafting solution, resulting in a somewhat higher Si/Al molar ratio of 16.8 ± 0.4 (3.5 wt % Al) in the functionalized film. Dissolution of the small amount of aluminosilica resulted from cleavage of some Si−O−Al bonds, due to interactions with the perfluorosulfonic-acid species under the relatively high temperature (110 °C) PFSA-grafting conditions used. By comparison, no significant loss of aluminum (Si/Al = 16.9 ± 0.2) was observed during the subsequent backfilling of the mesopores with 4 M triflic acid at room temperature. The resulting functionalized film contained 8 wt % triflic acid within the mesopores.

Quantitative single-pulse ^{27}Al MAS NMR spectra of cubic mesoporous PFSA- and aluminosilica-functionalized films are consistent with the bulk elemental analyses and provide insights into the coordination and relative and absolute concentrations of the different types of aluminosilica moieties in the films. For example, 1D single-pulse ^{27}Al MAS NMR spectra (Supporting Information, Figure S4a) of a powder obtained from a aluminosilica-functionalized film containing 3.7 wt % Al (Si/Al = 15.6) shows two ^{27}Al signals, whose chemical-shifts of 56 and 9 ppm are consistent with four- and six-coordinate aluminosilica species, respectively,[70] the latter of which interacts strongly with adsorbed water, as established by 2D ^{27}Al{^{1}H} HETCOR NMR (Supporting Information, Figure S5). In addition, integration of the peak areas establishes that 92% of the aluminosilica sites are four-coordinated (Table 1). It is noteworthy that, compared to elemental analysis results, over 90% of the total aluminum atoms in the material are accounted for in the single-pulse ^{27}Al MAS spectrum by using a known mass of AlN as an internal spin-counting standard. Similar quantitative analyses of ^{27}Al MAS NMR spectra (Supporting Information, Figure S4b,c) for the cubic mesoporous PFSA-grafted aluminosilica film (5 wt % PFSA, 3.5 wt % Al), prior to and after backfilling with triflic acid, establish that the perfluorosulfonic-acid functionalization step converts a substantial additional fraction of the framework aluminosilica species from four-coordinate $^{27}Al^{IV}$ to six-coordinate $^{27}Al^{VI}$ species, with the latter increasing from 8% to 61% $^{27}Al^{VI}$. This trend continues upon incorporation of 8 wt % triflic acid into the mesopores of otherwise identical cubic mesoporous PFSA- and aluminosilica-grafted films, resulting in a dominant ^{27}Al signal at 3 ppm corresponding to six-coordinate $^{27}Al^{VI}$ species (99%), while the signal at 56 ppm associated with four-coordinate $^{27}Al^{IV}$ moieties has almost completely disappeared (Table 1). The increase in coordination of the surface aluminosilica moieties is due to strong interactions with adsorbed water and/or triflic acid species,[71] as will be shown and discussed in detail below.

Molecular Surface Interactions. The local compositions, structures, and surface interactions of the various molecular species present in PFSA-grafted mesoporous aluminosilica films with triflic-acid-filled pores are central to their macroscopic proton conduction properties. Such molecular-level insights can be established through the use of 2D heteronuclear chemical-shift correlation (HETCOR) NMR measurements that rely on dipolar couplings between ^{1}H or ^{19}F and ^{29}Si or ^{27}Al nuclei for site-specific information on where functional species are grafted or adsorbed. In particular, the molecular proximities of proton- or fluorine-containing species (e.g., water, perfluorosulfonic acid, or triflic acid) to specific ^{29}Si or ^{27}Al moieties associated with the inorganic framework can be definitively distinguished and subsequently correlated with macroscopic water retention and proton conduction properties of the membrane materials.

Solid-state 2D NMR analyses provide detailed information on local compositions and molecular-level structures in acid-functionalized mesoporous aluminosilica films, particularly with respect to surface grafting and adsorption sites in the mesopore channels. For example, 2D ^{29}Si{^{1}H} HETCOR NMR spectra correlate interactions between dipole−dipole-coupled proton moieties (e.g., adsorbed water and surface hydroxyl groups) and framework ^{29}Si sites in functionalized mesoporous films. Figure 2a shows a 2D ^{29}Si{^{1}H} HETCOR spectrum acquired at −30 °C for PFSA-grafted (5 wt % PFSA) cubic mesoporous aluminosilica (3.5 wt % Al) containing 8 wt % triflic acid in the mesopores. Separately acquired quantitative single-pulse ^{29}Si and ^{1}H MAS spectra are plotted along the corresponding axes of the

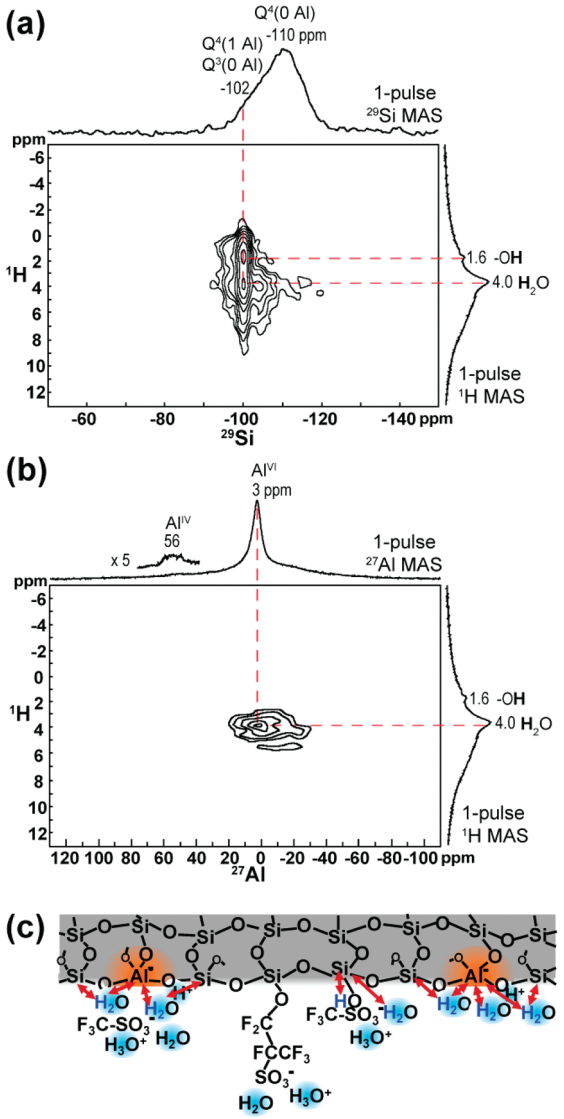

Figure 2. Solid-state 2D (a) $^{29}Si\{^{1}H\}$ and (b) $^{27}Al\{^{1}H\}$ HETCOR NMR spectra acquired at −30 °C (6 kHz MAS) for the same cubic mesoporous PFSA-grafted aluminosilica (5 wt % PFSA, 3.5 wt % Al) film containing 8 wt % CF_3SO_3H acid in the mesopores, as in Table 1 (bottom). Separate single-pulse 1D ^{29}Si, ^{27}Al, and ^{1}H MAS NMR spectra acquired at −30 °C are plotted along their corresponding axes. (c) Schematic diagram depicting the interactions (red arrows) of water and hydroxyl species with surface ^{29}Si or ^{27}Al moieties in the aluminosilica framework, as established by the 2D NMR spectra.

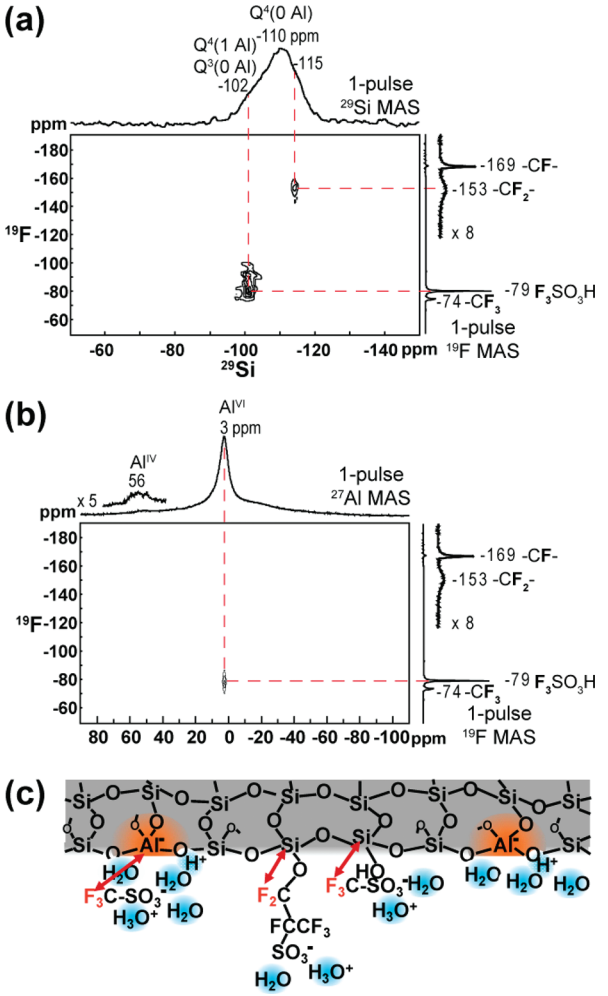

Figure 3. Solid-state 2D (a) $^{29}Si\{^{19}F\}$ and (b) $^{27}Al\{^{19}F\}$ HETCOR NMR spectra acquired at −30 °C (6 kHz MAS) for the same PFSA-grafted cubic mesoporous aluminosilica (5 wt % PFSA, 3.5 wt % Al) films containing 8 wt % CF_3SO_3H, as examined in Figure 2 and Table 1 (bottom). Separate single-pulse 1D ^{29}Si, ^{27}Al, and ^{19}F MAS NMR spectra are plotted along their corresponding axes. (c) Schematic diagram depicting the selective interactions (red arrows) of grafted PFSA and triflic acid species with surface ^{29}Si or ^{27}Al moieties, respectively, in the aluminosilica framework, as established by the 2D NMR spectra.

2D HETCOR contour plot, so that all of the resonances are accounted for, even if they do not contribute intensity correlations in the 2D spectrum. The 1D ^{29}Si MAS spectrum along the horizontal axis in Figure 2a confirms the presence of two broad overlapping ^{29}Si signals, whose chemical shifts of −102 and −110 ppm are consistent with incompletely condensed Q^3 and fully cross-linked Q^4 ^{29}Si sites in the silica framework.[72] The peak at −102 ppm is expected also to have an additional contribution from fully cross-linked ^{29}Si sites that have one ^{27}Al nearest neighbor (bonded via bridging oxygen atoms), denoted as Q^4(1 Al) sites.[72] The single-pulse ^{1}H MAS spectrum displayed along the vertical axis in Figure 2a shows two broad ^{1}H signals, corresponding to surface hydroxyl groups (1.6 ppm, 2 ppm full-width-half-maximum, fwhm) and adsorbed water (4.0 ppm, 3 ppm fwhm). The breadth of the overlapping peaks is due principally to strong homonuclear $^{1}H-^{1}H$ dipolar couplings,[73] which are incompletely averaged under the temperature and MAS conditions used. The 2D $^{29}Si\{^{1}H\}$ HETCOR contour plot (Figure 2a) shows strong correlated signal intensity at 1.6 ppm in the ^{1}H dimension and −102 ppm in the ^{29}Si dimension, which is ascribed to hydroxyl groups directly bonded to Q^3 ^{29}Si sites. In addition, 2D signal intensity at 4.0 ppm in the ^{1}H dimension and −102 ppm in the ^{29}Si dimension can arise from polarization transfer between adsorbed water protons and either hydrogen-bonded Q^3 ^{29}Si silanol species or Q^4(1 Al) ^{29}Si moieties adjacent to neighboring aluminum atoms grafted onto the framework surface.

More importantly, strong interactions exist between ^{1}H species associated with adsorbed water and framework ^{27}Al

dx.doi.org/10.1021/ja2038529 |J. Am. Chem. Soc. 2011, 133, 16023–16036

aluminosilica sites.[58] These are established by the 2D $^{27}Al\{^{1}H\}$ HETCOR spectrum in Figure 2b for the same PFSA-grafted (5 wt % PFSA) cubic mesoporous aluminosilica (3.5 wt % Al) material containing 8 wt % triflic acid also acquired at −30 °C. A separately acquired single-pulse 1D ^{27}Al MAS spectrum along with the same ^{1}H MAS spectrum as in Figure 2a are displayed along the corresponding axes of the 2D $^{27}Al\{^{1}H\}$ HETCOR contour plot in Figure 2b. The single-pulse ^{27}Al MAS spectrum reveals a sharp intense signal at 3 ppm and only a hint of a very weak signal at 56 ppm, which are attributed to predominant (99%) six-coordinate $^{27}Al^{VI}$ and virtually absent (1%) four-coordinate $^{27}Al^{IV}$ species, respectively (Table 1, bottom). Notably, the 2D contour plot of the $^{27}Al\{^{1}H\}$ HETCOR spectrum contains a dominant 2D intensity correlation at 3 ppm in the ^{27}Al dimension and 4.0 ppm in the ^{1}H dimension. This strong 2D signal intensity originates from strong dipole−dipole couplings between the six-coordinate framework $^{27}Al^{VI}$ aluminosilica species and spatially proximate protons of adsorbed water molecules.[74] Figure 2c depicts the strong interactions between hydroxyl groups and adsorbed water with silanol and grafted aluminosilica surface species, respectively, reflecting the enhanced hydrophilicity of the mesopores that accounts for the higher water retention properties of the functionalized material.

Similar, but more selective interactions are observed for the proton-conducting moieties, namely, the covalently grafted PFSA and adsorbed triflic acid species, at different framework silica and/or aluminosilica sites in the functionalized films. Analogous 2D $^{29}Si\{^{19}F\}$ and $^{27}Al\{^{19}F\}$ HETCOR spectra in Figure 3a,b acquired for the same PFSA-grafted (5 wt % PFSA) cubic mesoporous aluminosilica (3.5 wt % Al) film material with 8 wt % triflic acid in the mesopores elucidate specific surface grafting or adsorption sites of the perfluorosulfonic-acid and triflic acid species. In particular, Figure 3a shows the 2D $^{29}Si\{^{19}F\}$ HETCOR spectrum, together with separately acquired single-pulse 1D ^{29}Si and ^{19}F MAS spectra along the horizontal and vertical axes, respectively. The three ^{19}F signals at −169, −153, and −74 ppm have isotropic chemical shifts and integrated-intensity ratios that are consistent with the relative stoichiometries (1:2:3) of the −CF−, $-CF_2-$, and $-CF_3$ fluorine moieties, respectively, of grafted perfluorosulfonic acid species.[40] The narrow signal at −79 ppm in the ^{19}F MAS spectrum is from the methyl fluorine atoms of the triflic acid (CF_3SO_3H) species.[77] An identical single-pulse ^{19}F MAS spectrum is obtained for the PFSA-grafted cubic mesoporous aluminosilica film material prior to backfilling with triflic acid (Supporting Information, Figure S6), except that, unsurprisingly, the narrow peak at −79 ppm is not present. In the 2D $^{29}Si\{^{19}F\}$ HETCOR spectra of PFSA-grafted cubic mesoporous aluminosilica film materials with (Figure 3a) and without (Supporting Information, Figure S6) triflic acid backfilling the mesopores, correlated 2D signal intensity is observed at −153 ppm in the ^{19}F dimension and −115 ppm in the ^{29}Si dimension, establishing that the perfluorosulfonic-acid species are grafted through their $-CF_2-$ groups to the mesopore silica surfaces, consistent with the configuration suggested by Alvaro et al.[40]

The covalently grafted PFSA moieties interact strongly with the silica mesochannel surfaces, significantly affecting local ^{29}Si electronic environments. In particular, the position of the ^{29}Si signal at −115 ppm is noteworthy, as it is shifted to a much lower frequency than typically observed for Q^3 ^{29}Si sites (ca. −102 ppm) to which the $-CF_2-$ perfluorosulfonic-acid moieties are expected to be grafted. In fact, the signal is displaced to lower frequency than even fully condensed Q^4 ^{29}Si species, which usually appear near −110 ppm. The nature of these interactions between the ^{29}Si grafting sites and PFSA moieties is elucidated by density functional theory (DFT) calculations, which allow the ^{29}Si isotropic chemical shifts of different $^{29}Si-O-CF_2-$ moieties to be calculated for atom-cluster models. An example of one such cluster (**I**) is shown in Figure 4, which depicts a surface silicon atom Si(1) as an initially ungrafted Q^3 ^{29}Si silanol site in the silica network, along with first- (including one Q^3 and two Q^4 ^{29}Si atoms) and second- (H-terminated) nearest-neighbor Si atoms that are four-coordinated to bridging oxygen atoms.[68]

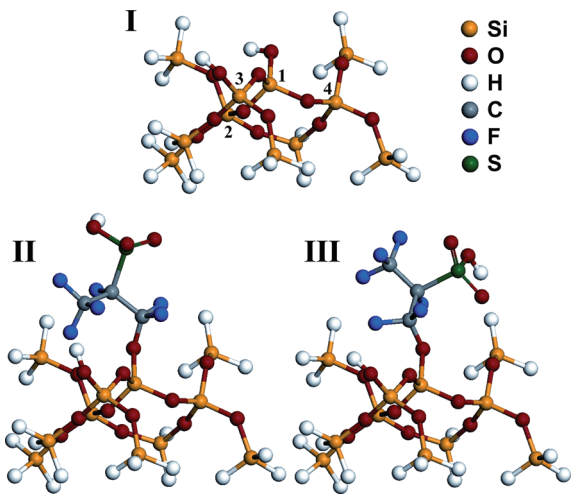

Figure 4. Molecular clusters used to model the grafting of perfluorosulfonic acid moieties (PFSA) on a silica surface and for associated DFT calculations of ^{29}Si isotropic chemical shifts: (**I**) a surface Q^3 ^{29}Si site Si(1) shown in a $[Si_{10}O_{12}H_{21}]Si-OH$ cluster before and (**II** and **III**) after substitution of the −OH group by a −PFSA−H moiety with different initial conformations and after subsequent relaxation of the grafted moiety, including grafting O and terminal H atoms.

The effect of covalently grafting perfluorosulfonic acid species at Q^3 silica sites can be modeled by replacing the silanol group initially present in cluster **I** by $-OCF_2CF(CF_3)(SO_3H)$ (i.e., "−PFSA−H") in various initial conformations.[78] Partial optimization of the grafted PFSA moiety, including O atoms at the grafting site and the terminal H atoms of the silica cluster, with other O and Si atomic positions frozen, led to clusters **II** and **III** (Figure 4). Subsequent DFT calculations for clusters **II** and **III** yielded values for the respective ^{29}Si isotropic chemical shifts that are associated with the local environments of the Si grafting site and Si nearest neighbors in each of the different clusters. As shown in Table 2, the calculations predict isotropic ^{29}Si chemical shift values of between −110 and −114 ppm for the grafting site Si(1), reflecting displacements of −8 to −12 ppm to lower frequencies, depending upon the conformation of the grafted of PFSA moiety. Such displacements are attributed to through-bond interactions of the $-CF_2-$ moiety that increase electron density at the Q^3 ^{29}Si grafting site. These results are in good agreement with the appearance of the ^{29}Si signal at −115 ppm, which is strongly correlated in the 2D $^{29}Si\{^{19}F\}$ HETCOR spectrum (Figure 3a) with the ^{19}F signal at −153 ppm from the PFSA $-CF_2-$moieties. Consequently, this ^{29}Si signal can be confidently assigned to $Q^4(1\ CF_2)$ ^{29}Si moieties that are displaced

Table 2. Calculated Isotropic ^{29}Si NMR Chemical Shifts for Different $[Si_{10}O_{12}H_{21}]Si-O-X$ Clusters, with X = H or −PFSA−H in Different Conformations

		^{29}Si isotropic chemical shift (ppm)[a]				signal displacement relative to **I** (ppm)			
cluster	cluster composition	Si(1) (Q^3)	Si(2) (Q^3)	Si(3) (Q^4)	Si(4) (Q^4)	Si(1) (Q^3)	Si(2) (Q^3)	Si(3) (Q^4)	Si(4) (Q^4)
I	$[Si_{10}O_{12}H_{21}]Si-OH$	−102	−105	−105	−113	-	-	-	-
II	$[Si_{10}O_{12}H_{21}]Si-O-PFSA-H$	−114	−105	−105	−113	−12	0	0	0
III	$[Si_{10}O_{12}H_{21}]Si-O-PFSA-H$	−110	−105	−106	−113	−8	0	−1	0
	Average of **II** and **III**	−112	−105	−106	−113	−10	0	−1	0

[a] ^{29}Si chemical shifts are given relative to TMS using the chemical shift calculation conducted on cluster **I** (Fig. 4) as a secondary reference. The DFT calculations yield shielding values σ_{calc} that are converted to chemical shifts δ_{calc} using the expression $\delta_{calc} = \sigma_{ref} - \sigma_{calc} + \delta_{ref}$, where σ_{ref} is the average of the four shielding values for each Si site in cluster **I** (two Q^3 and Q^4 moieties), and $\delta_{ref} = -106$ ppm is the average of the experimental shifts for two Q^3 moieties (−102 ppm) and two Q^4 moieties (−110 ppm).

by ca. −13 ppm with respect to ungrafted Q^3 sites at ca. −102 ppm. Furthermore, the DFT calculations establish that the Q^4 and Q^3 ^{29}Si sites adjacent to the grafting site are only weakly affected (displacements <1 ppm, Table 2) by their proximities to the grafted $-CF_2-$ groups; no evidence of strong interactions between the PFSA fluorine atoms and the silicon atoms adjacent to the grafting site was observed in the geometry optimizations. This is consistent with the absence of correlated signal intensity between the $-CF_2-$ moieties and nongrafted Q^4 or Q^3 ^{29}Si sites (at ca. −110 or −102 ppm, respectively), due to inefficient ^{29}Si{^{19}F} cross-polarization associated with mobile, distant, and/or conformationally disordered PFSA moieties. The DFT calculations, in conjunction with 2D ^{29}Si{^{19}F} NMR measurements, thus yield detailed insights on the local molecular environments of the PFSA-functionalized silica grafting sites.

By comparison, triflic acid species interact with *ungrafted* Q^3 silanol and/or Q^4(1 Al) ^{29}Si moieties at the functionalized mesopore channel surfaces. This is evident in the 2D ^{29}Si{^{19}F} HETCOR spectrum (Figure 3a) for the PFSA-grafted cubic mesoporous aluminosilica film containing 8 wt % triflic acid, which exhibits strong correlated 2D signal intensity at −79 ppm in the ^{19}F dimension and −102 ppm in the ^{29}Si dimension, corresponding to $-CF_3$ triflic acid moieties interacting with framework Q^3 or Q^4(1 Al) ^{29}Si sites. The high mobility of triflic acid species at room temperature required that the measurement be conducted at −30 °C to enhance magnetization transfer between the ^{19}F nuclei and ^{29}Si species in the inorganic framework. Such correlated signal intensity reflects adsorption of triflic acid, for example, through hydrogen bonding or electrostatic interactions, at Q^3 silanol sites or near (<1 nm) an aluminosilica Q^4(1 Al) ^{29}Si moiety, which exhibit similar ^{29}Si isotropic chemical shifts. These results are consistent with weaker interactions between the adsorbed and more mobile triflic acid species at surface sites, compared to the covalently grafted PFSA moieties.

2D ^{27}Al{^{19}F} HETCOR NMR results similarly provide detailed and complementary information on how the different fluorine species interact with framework aluminosilica moieties. The 2D ^{27}Al{^{19}F} HETCOR spectrum shown in Figure 3b for the same PFSA-grafted cubic mesoporous aluminosilica (5 wt % PFSA, 3.5 wt % Al) film material containing 8 wt % triflic acid shows only a single 2D intensity correlation at −79 ppm in the ^{19}F dimension and 3 ppm in the ^{27}Al dimension, which corresponds to interactions between the fluorine atoms of adsorbed triflic acid moieties and six-coordinate aluminosilica ^{27}Al mesopore surface sites. As for the 2D ^{29}Si{^{19}F} HETCOR spectrum, the ^{27}Al{^{19}F} HETCOR measurement was also conducted at −30 °C to reduce the mobility of the triflic acid species and enhance ^{19}F−^{27}Al cross-polarization. By comparison, the $-CF_2-$ fluorine atoms of the grafted perfluorosulfonic acid species cross-polarize efficiently at room temperature to ^{29}Si framework moieties in the mesopore channels, consistent with the PFSA functional groups being covalently bonded to the mesopore walls and thus less mobile. At relevant PEM fuel cell operating temperatures (T > 60 °C), the triflic acid species will be highly mobile and contribute to the enhanced conductivity of ions within the mesopore channels of PFSA-functionalized films, while the PFSA moieties will remain anchored to the mesopore walls. In contrast to the 2D ^{29}Si{^{19}F} HETCOR results (Figure 3a), the absence of any correlated signal intensity in the 2D ^{27}Al{^{19}F} HETCOR spectrum associated with the perfluorosulfonic-acid species (at −169, −153, or −74 ppm in the ^{19}F dimension) establishes unambiguously that the perfluorosulfonic-acid species are only grafted to the mesopore surfaces at Q^4(1 CF_2) ^{29}Si sites, which were formerly Q^3 silanol moieties. Figure 3c summarizes the selective interactions of grafted PFSA and adsorbed triflic acid species with surface ^{29}Si or ^{27}Al moieties, respectively, in the aluminosilica framework, as established by the 2D NMR spectra. This is consistent with observations by Alvaro et al.,[40] which reported grafting of PFSA species onto silica, but without coexisting aluminosilica sites. The 2D ^{27}Al{^{1}H} and ^{27}Al{^{19}F} HETCOR results (Figures 2b and 3b) furthermore establish that the transformation of initially four-coordinate framework Al species into Al^{VI} species is due principally to strong surface interactions with adsorbed water and possible contributions from triflic acid species. The 2D HETCOR NMR and modeling results thus provide comprehensive insights on site-specific interactions among the various grafted and/or adsorbed functional moieties at distinct framework surface sites.

Optimization of Mesopore Functionalities. The selective grafting of perfluorosulfonic-acid species onto surface silica sites suggests that the proton conductivity properties at elevated temperatures can be improved by collectively optimizing the aluminosilica and PFSA grafting densities on the interior mesopore surfaces. As discussed previously, maximum hydrophilicity is obtained at the highest aluminosilica surface coverages. However, in this case, the number of surface silanol sites available for PFSA grafting is significantly reduced (and mesostructural ordering potentially diminished), leading to relatively low proton conductivities, independent of temperature or

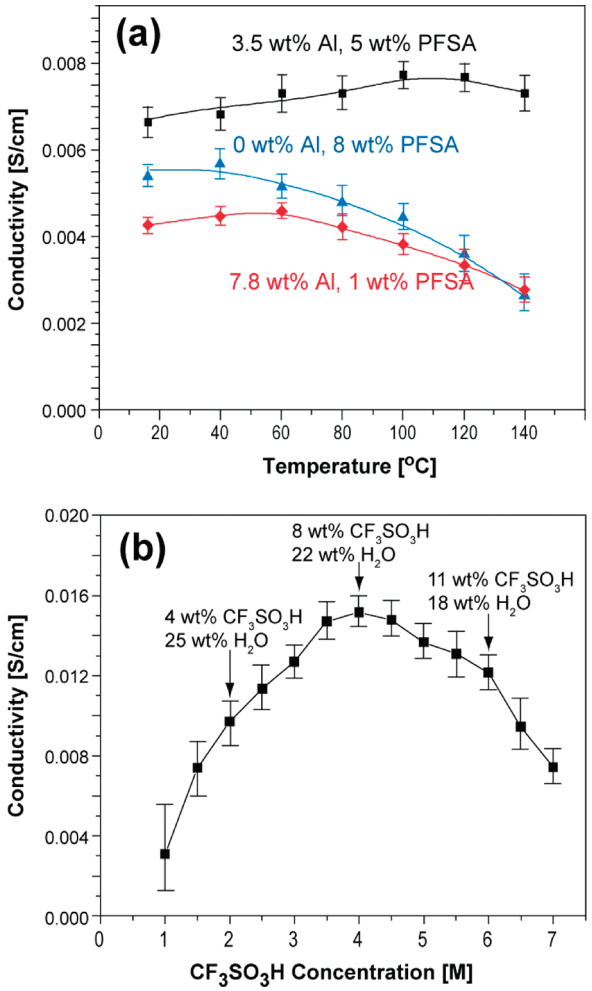

Figure 5. Optimization of aluminosilica- and PFSA-grafting concentrations and triflic-acid mesopore-filling concentrations in cubic mesoporous silica films. (a) Proton conductivities as a function of temperature at 50% relative humidity (R.H.) for identical 65-μm-thick cubic mesoporous silica films containing different concentrations of surface-grafted aluminosilica (Al) and perfluorosulfonic-acid (PFSA) moieties: [blue triangles] 0 wt % Al, 8 wt % PFSA; [black squares] 3.5 wt % Al, 5 wt % PFSA; or [red diamonds] 7.8 wt % Al, 1 wt % PFSA. (b) Proton conductivity as a function of mesopore-filling triflic acid concentrations in free-standing 105-μm-thick 5 wt % PFSA- and 3.5 wt % Al aluminosilica-grafted cubic mesoporous silica films at ambient conditions (20 °C and ~40% R.H.).

humidity. Similarly, high loadings of grafted proton-conducting PFSA species are achieved with high surface silanol concentrations and low aluminosilica coverages, although this leads to significantly lower material hydrophilicity, lower water retention, and thus also relatively low proton conductivities at elevated temperatures or low humidities. Consequently, it is necessary to optimize the mesopore surface compositions to allow for a high concentration of grafted perfluorosulfonic-acid species, while maintaining highly hydrophilic aluminosilica surface environments within the mesopore channels.

Using the insights provided by 2D NMR, we hypothesized that proton conductivities could be enhanced at elevated temperatures and/or lower humidities by balancing the aluminosilica and PFSA contents of the materials. This was tested by synthesizing otherwise identical cubic mesoporous films under identical conditions, except for altering the aluminosilica and PFSA loadings of the materials (initially, in the absence of additional triflic acid in the mesopores, which will be discussed below). Specifically, film materials with a range of aluminosilica surface coverages were examined: calcined cubic mesoporous silica (0 wt % Al) and cubic mesoporous aluminosilica with 3.5 or 7.8 wt % Al, corresponding to ca. 35% or 85% silanol coverages, respectively (see Materials and Methods). Each of these films was subsequently grafted with PFSA surface moieties under identical conditions to obtain loadings of 8, 5, or 1 wt % PFSA, corresponding to silanol coverages of approximately 90%, 55%, and 10%, respectively. As discussed above (Figure 1), silanol coverages by aluminosilica species above 85% are possible and higher aluminosilica concentrations achievable, though with degradation of mesostructural ordering in the film. Additionally, the alkaline-soluble alumina species compete with nonaqueous-soluble PFSA species for surface silanol groups in the sequential grafting treatments. Consequently, increased aluminosilica surface densities can be achieved in the mesopore channels, though at the expense of reducing the perfluorosulfonic-acid surface concentrations. Thus, the two must be optimized together to maximize the proton conductivity properties of the functionalized film materials at elevated temperatures or low humidities.

For example, Figure 5a shows plots of proton conductivity, measured as functions of temperature at 50% relative humidity, for three otherwise identical cubic mesoporous silica films that were functionalized with different aluminosilica and perfluorinated-sulfonic-acid surface-grafting densities. If no hydrophilic surface aluminosilica species are incorporated (0 wt % Al), a maximum amount of PFSA species (8 wt %) can be grafted onto the silica mesopore surfaces, leading to maximum proton conductivities (Figure 5a, blue triangles) of ca. 5.7×10^{-3} S/cm at 40 °C. Above this temperature, the conductivity values diminish rapidly, consistent with the low water retention[44] of the non-aluminosilica-containing materials that leads to low proton mobilities. In the other limit, for a maximum amount of hydrophilic aluminosilica (7.8 wt % Al) species incorporated onto the mesopore surfaces and the remaining silanol groups grafted with PFSA (1 wt %), a maximum proton conductivity of approximately 4.5×10^{-3} S/cm was measured at 60 °C (Figure 5a, red diamonds). This lower value reflects the lower concentration of proton-conducting moieties present, as a result of competitive consumption of surface silanol species by the aluminosilica grafting moieties. At higher temperatures, significantly lower conductivities are also observed, with both PFSA-only grafted (8 wt % PFSA) silica and high aluminosilica (7.8 wt% Al, 1 wt % PFSA) cubic mesoporous films displaying comparable conductivity values between 60 and 140 °C. For functionalized cubic mesoporous films containing aluminosilica and PFSA loadings between these two limits, proton conductivities were measured and could be enhanced at intermediate levels of the two functional components.

By balancing the need for both high hydrophilicity and strong acidity, aluminosilica and perfluorosulfonic-acid surface-grafting densities were co-optimized in multifunctionalized films, according to their temperature- and humidity-dependent proton-conduction properties. Specifically, a cubic mesoporous film with aluminosilica and PFSA contents of 3.5 wt % Al and 5 wt % PFSA (corresponding to ca. 35% and 55% silanol coverages, respectively) yielded the highest proton conductivity values at all of the temperatures and humidities examined (Figure 5a, black squares).

dx.doi.org/10.1021/ja2038529 |J. Am. Chem. Soc. 2011, 133, 16023–16036

Maximum conductivity values of ca. 7.7×10^{-3} S/cm were measured over the range 100−120 °C and persisted above 6.0×10^{-3} S/cm up to approximately 140 °C. Optimization of the bulk proton conductivities of the functionalized films to this extent was directly enabled by understanding the competitive molecular interactions at the various hydrophilic- and acidic-grafting sites within the mesopore channels and at their heterogeneous interfaces.

Proton conductivities of the acid-functionalized cubic mesoporous aluminosilica films are functions of temperature and relative humidity, as well as the concentration of perfluorosulfonic-acid species within the mesopore channels. While covalently grafted perfluorosulfonic-acid moieties allow for proton transport along the mesopore surfaces, additional ion conduction capacity through the membranes can be obtained by increasing the concentration of fluorosulfonic-acid moieties in the films by incorporating triflic acid (CF_3SO_3H) or other proton conducting species into the remaining mesopore volumes. This can be achieved by contacting the mesoporous films (silica, aluminosilica, and/or PFSA-grafted) with an aqueous solution of triflic acid, the concentration of which can be increased to increase the CF_3SO_3H-loading in the mesopores. While one might think that proton conductivity could be maximized by incorporating the highest concentrations of acid into the mesopores, this turns out not to be the case. Rather, intermediate pore-volume concentrations of triflic acid were found to yield higher proton conductivities in PFSA-grafted cubic mesoporous aluminosilica films, reflecting an additional and important underlying optimization criterion to the competitive silanol grafting constraints discussed above.

Similar to the approach above, the influence of mesopore-filling acid species (e.g., triflic acid) on the proton conductivity properties of otherwise identical perfluorosulfonic-acid- and aluminosilica-grafted mesoporous silica films was optimized in accordance with the molecular insights provided by solid-state 2D NMR (Figures 2 and 3). In Figure 5b, proton conductivity at 20 °C is plotted as a function of mesopore-filling triflic acid concentrations in 5 wt % PFSA and 3.5 wt % Al aluminosilica-grafted cubic mesoporous silica films. Functionalized films soaked in 0, 2, 4, or 6 M aqueous triflic acid solutions were measured to contain 0, 4, 8, and 11 wt % triflic acid, respectively, in the mesopores after air-drying. At low triflic acid concentrations, low conductivity values result at 20 °C (e.g., 9.7×10^{-3} S/cm for 4 wt % CF_3SO_3H obtained using 2 M triflic acid), due to inherently low acidic proton concentrations in the mesochannels. As the concentration of triflic acid in the mesopores is increased (by contact with more concentrated CF_3SO_3H solutions), the proton conductivity increased to a maximum value of 1.5×10^{-2} S/cm for 8 wt % triflic acid (4 M CF_3SO_3H). At still higher concentrations of triflic acid, however, significantly lower proton conductivities were observed. Importantly, these measurements are additionally correlated with the concentration of coexisting water in the mesopores, which fills the remaining free mesopore volume and which decreased steadily at higher triflic acid loadings. (Unlike many polymeric membrane materials, the mesoporous aluminosilica films do not swell.) Separate TGA/mass spectrometry measurements establish that, at 20 °C, identical films with 4, 8, and 11 wt % CF_3SO_3H in the mesopores possess water loadings of 25, 22, and 18 wt % H_2O, respectively. These results are consistent with initially higher concentrations of triflic acid providing correspondingly greater numbers of acidic protons in the mesoscale channels, with the balance of the mesopore volume occupied by water that facilitates mobility of the H^+ cations. As the concentration of triflic acid is increased, and along with it the concentration of acidic protons, the amount of residual mesopore volume available to water diminishes, eventually to a point (>8 wt %) where proton mobility and thus proton conductivity also begin to diminish. Similar results are obtained at elevated temperatures (up to 140 °C) (Supporting Information Figure S7). Thus, the existence of optimal concentrations of functional species in the mesoporous films for which maximum proton conductivity is observed is likely a consequence of the competing effects of higher densities of strong acid sites in the mesopore channels being offset by reduced local hydration of the triflic acid species[79] and resulting diminished proton mobilities.[80]

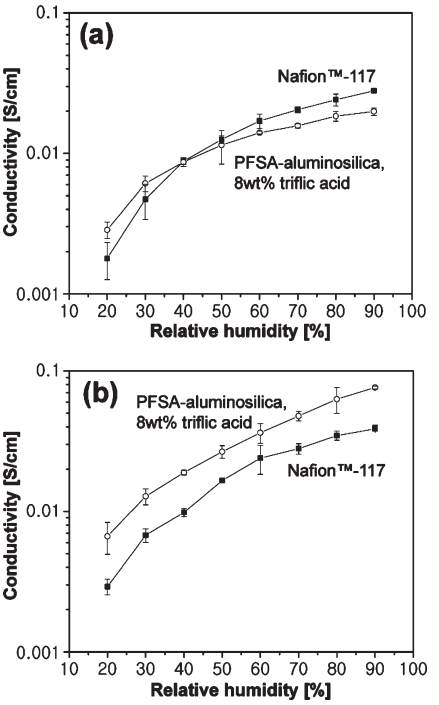

Figure 6. Proton conductivities measured as functions of relative humidity at (a) 80 °C and (b) 120 °C for an optimized 180-μm-thick cubic mesoporous perfluorosulfonic-acid-grafted aluminosilica (5 wt % PFSA, 3.5 wt % Al) film containing 8 wt % triflic acid [○] and for a Nafion 117 membrane [■].

For comparison, proton conductivity values as functions of relative humidity (R.H.) at 80 and 120 °C under otherwise identical measurement conditions are shown in Figure 6 for the collectively optimized PFSA-grafted cubic mesoporous aluminosilica (3.5 wt % Al, 5 wt % PFSA) film containing 8 wt % triflic acid and a commercial perfluorinated-sulfonic-acid polymer (Nafion 117) film. At 80 °C and high relative humidities, Nafion 117 membranes typically manifest near-maximum proton conductivity performance.[81] Under these conditions, as shown in Figure 6a, the functionalized mesostructured film exhibits proton conductivities comparable to, but modestly lower than Nafion 117. The H^+ conductivities of both materials are diminished at lower humidity levels, where dehydration effects are exacerbated. However, the proton conductivity of the optimized mesostructured film is more stable, showing less change across a broad humidity range and being higher at low humidity levels. As the relative humidity is decreased, the proton conductivity of

Nafion 117 rapidly diminishes to values of $\sim 2 \times 10^{-3}$ S/cm at 20% R.H. In contrast, the optimized PFSA-grafted aluminosilica film containing 8 wt % triflic acid in the mesopores exhibits relatively moderate decreases in proton conductivity values (3×10^{-3} S/cm at 20% R.H.). Compared to Nafion 117 at 80 °C, the functionalized mesostructured film exhibits higher proton conductivities, at relative humidities below 40%.

At higher temperatures, for example, 120 °C (Figure 6b), both Nafion and the optimized cubic mesoporous PFSA-aluminosilica materials show enhanced proton conductivities compared to their properties at 80 °C, though the latter significantly more so. For Nafion 117, the increased intrinsic mobility of protons at the higher temperature is offset by channel closure to increasing extents, due to membrane dehydration at higher temperatures or lower humidities. In contrast, the connectivities and dimensions of the aluminosilica mesochannels are independent of temperature or relative humidity for the range of conditions examined and thus remain open and robust. As a result, at 120 °C, the optimized mesostructured film shows higher conductivities than Nafion 117 over the entire range of humidity conditions investigated, from 20 to 90%.

The different temperature-dependences associated with proton transport in the multiply functionalized and Nafion membranes can be quantified by evaluating and comparing the apparent activation energies that characterize their ion-conduction kinetics. Such activation energies include contributions from intrinsic barriers to proton hopping and include effects associated with solvent species, counter-anions, and surfaces, along with channel constrictions in the case of Nafion. The apparent activation energies (E_a) of the cubic mesoporous PFSA-aluminosilica functionalized membranes with and without triflic acid and Nafion 117 were determined by measuring their proton conductivities (σ) as functions of temperature and humidity and fitting the results to a linearized form of the Arrhenius equation $\sigma = \sigma_0 \exp(-E_a/RT)$ (Supporting Information, Figure S8). The resulting fits were linear for the different materials over the temperature range of 80−120 °C at 100% and 50% relative humidities. Accordingly, the apparent activation energy associated with proton conduction of Nafion 117 at 100% relative humidity was found to be 11 kJ/mol, which is in good agreement with literature values that range from 10 to 15 kJ/mol.[82−84] At a reduced relative humidity (50%), lower values were obtained for both the proton conductivity (Figure 6) and the apparent activation energy (8.1 kJ/mol). Under such conditions, higher activation energies might be anticipated, which would indicate more strongly associated H^+ cations at the sulfonic acid moieties as the water content diminishes.[84] However, thermally induced or hydration-dependent structural changes,[85] for example, crystallization of the polymer backbone[86] or closure of the ion-conducting channels can occur, resulting in reduced proton conductivities of wholly polymeric membrane materials at elevated temperatures and reduced humidities. Consequently, decreased overall mobilities and/or continuities of the ion-conducting moieties eventually offset otherwise enhanced intrinsic ion-exchange kinetics at elevated temperatures.

By comparison, the apparent activation energy for proton transport in a PFSA-functionalized cubic mesoporous aluminosilica (5 wt % PFSA, 3.5 wt % Al, no triflic acid) membrane at 50% relative humidity was measured to be 5.3 kJ/mol, which is lower than that of Nafion 117. This is consistent with the higher water retention and robustness of the aluminosilica mesochannels in the multiply functionalized membranes, which result in greater

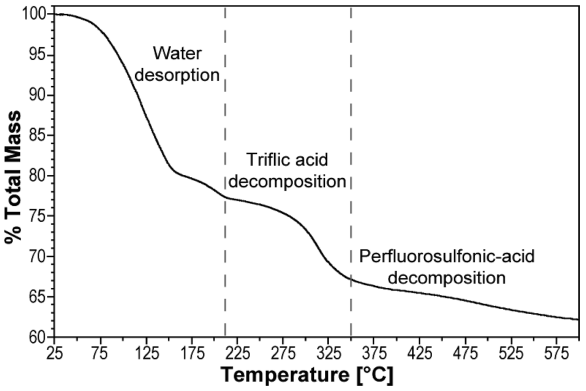

Figure 7. Thermogravimetric analysis (TGA) of a cubic perfluorosulfonic-acid-grafted mesoporous aluminosilica (5 wt % PFSA, 3.5 wt % Al) film containing 8 wt % triflic acid (CF_3SO_3H) in the mesopores. Species mass losses at different temperatures are determined from mass spectrometry analyses of the effluent gases (Supporting Information, Figure S9).

extents of H^+ dissociation from the sulfonic acid groups, as well as increased ion transport, at similar humidities (and higher temperatures). The presence of triflic acid in the mesopores increases the density of acid centers and can promote proton transport, provided that sufficient water remains present. For an otherwise identical cubic mesoporous PFSA- and aluminosilica-functionalized membrane containing 8 wt % triflic acid, a significantly higher activation energy of 22 kJ/mol is measured for proton conduction at 50% R.H. Such a high value is nevertheless nearly identical to the apparent activation energy calculated for proton transport in bulk aqueous solutions of hydrated triflic acid.[87] This suggests that the higher apparent activation energy measured for proton transport in the multiply functionalized triflic-acid-PFSA-aluminosilica membranes is due principally to viscosity effects, which are strongly temperature dependent (E_a = 26 kJ/mol),[87] in the nonswellable mesochannels of the hybrid material.

Finally, molecular interactions between adsorbed or grafted species and the heterogeneous framework affect not only the proton conductivity properties of the membranes, but also the thermal stabilities of the functional groups. Thermogravimetric analyses (TGA) conducted on the collectively optimized 5 wt % perfluorosulfonic-acid-grafted cubic mesoporous aluminosilica (3.5 wt % Al) films containing 8 wt % CF_3SO_3H establish the relative and absolute thermal stabilities of adsorbed water and the acid functional species within the mesopores. Mass spectrometry measurements were conducted simultaneously on the effluent gases from the materials as they were heated to identify the chemical species responsible for specific mass losses (Supporting Information, Figure S9). The TGA results in Figure 7 show an initial 23% mass loss between room temperature and 220 °C, which is attributed to adsorbed water within the mesopores. This establishes the significantly higher water retention of the multifunctionalized films, compared to Nafion.[44] The water retention of the film also can be represented by the mean number of water molecules per sulfonic acid group, denoted as λ, and for which the multifunctionalized mesostructured film is estimated from the TGA data to have a high value of 17 at 25 °C. Furthermore, relatively high water retention is maintained at elevated temperatures, as manifested by λ values of 15, 12, and 8 H_2O/$-SO_3H$ at 80, 100, and 120 °C, respectively, which are comparable to fully hydrated Nafion 117 ($\lambda \sim 14$, 100% R.H.) at room

temperature.[89,90] These bulk quantitative results are consistent with the molecular 2D $^{27}Al\{^{1}H\}$ HETCOR analyses (Figure 2), which showed a significant fraction of such water to be strongly bound at six-coordinate ^{27}Al aluminosilica sites in the framework. The next 8% mass loss that is observed (Figure 7) between 225 and 325 °C results from the depletion of triflic acid species that, despite their high mobility, nevertheless are strongly interacting and retained in the mesopores at these relatively high temperatures. Interestingly, the combined TGA/mass spectrometry measurements (Supporting Information, Figure S9) indicate that the low-molecular-mass CF_3SO_3H species decompose as they desorb from the mesopores, rather than doing so intact. Samples with differences in triflic acid concentration backfilling the mesopores lead to expected differences in mass losses over the temperature range 225−325 °C. Above 330 °C, mass loss (ca. 3%) is due to decomposition of covalently grafted perfluorosulfonic acid species, with no further mass reduction detected above 600 °C. These macroscopic conductivity and thermal stability results are correlated and consistent with the collective molecular-level optimizations and 2D NMR characterization of functional group compositions and structures in the heterogeneous mesoporous aluminosilica films.

CONCLUSIONS

Establishing the compositions, structures, distributions, and interfacial interactions of molecular species within multiply functionalized mesoporous materials permits substantial control over their macroscopic properties, specifically with respect to temperature- and humidity-dependent proton conductivities of functionalized films. Furthermore, such insights yield important molecular design and synthesis criteria that allow the incorporation and collective optimization of several coupled properties, even those that may rely on individually incompatible functionalization conditions. The use of a sequential synthesis protocol overcomes previously severe limitations to the incorporation of technologically promising combinations of functional properties, which have previously not been possible to introduce together in a single set of synthesis-processing conditions.

The large number of synthesis, composition, and structural variables and even larger number of possible combinations can be narrowed significantly by applying powerful methods of 2D NMR. 2D heteronuclear chemical-shift correlation NMR spectroscopy establishes selective and competitive molecular interactions in acid-functionalized mesoporous aluminosilica proton-exchange membrane materials. 2D $^{27}Al\{^{19}F\}$, $^{29}Si\{^{19}F\}$, $^{27}Al\{^{1}H\}$, and $^{29}Si\{^{1}H\}$ HETCOR results show unambiguously that perfluorosulfonic acid species are covalently grafted to the mesopore surfaces preferentially through silica sites and that pore-filling water and triflic acid species adsorb at ^{27}Al aluminosilica framework sites on the mesopore surfaces. These results in combination with complementary quantitative single-pulse NMR, small-angle X-ray diffraction, electron microscopy, thermogravimetric, adsorption, and elemental analyses provide a thorough understanding of the molecular and mesoscopic compositions and structures of the multiply functionalized materials and how they are correlated with bulk material properties, such as proton conductivity and thermal stability. The insights provided by these results have enabled optimized compositions, surface structures, mesopore connectivities, and stabilities to be established in novel inorganic−organic hybrid membranes that exhibit promising proton conduction properties, compared to wholly polymeric analogues. Additional device-related properties to be considered include the mechanical toughness of the materials and electro-osmotic transport of anions, water, or gas species during operation of resulting membrane-electrode assemblies. Improvements or optimization of these properties are addressable by using similar multistep functionalization protocols that are analogous to that described here and which are currently underway in our laboratory. The overall functionalization approach and understanding are general and expected to allow for similar optimizations of material compositions and film/membrane performances in a variety of applications, particularly in fuel cells and batteries for which multifunctional materials may present significant new property advantages and device opportunities.

ASSOCIATED CONTENT

Supporting Information. Detailed mesostructural characterization results from TEM, small-angle X-ray diffraction, and nitrogen sorption are provided for a perfluorosulfonic-acid-grafted mesoporous aluminosilica membrane prior to backfilling of the mesopores with triflic acid. In addition, a 2D $^{29}Si\{^{19}F\}$ HETCOR NMR spectrum is shown for a powder prepared from the perfluorosulfonic-acid-grafted cubic mesoporous aluminosilica film material prior to backfilling of the mesopores with triflic acid, showing unambiguous evidence for acid grafting to the aluminosilica surface through $^{19}F-^{29}Si$ heteronuclear dipole−dipole couplings. This material is available free of charge via the Internet at http://pubs.acs.org.

AUTHOR INFORMATION

Corresponding Author
bradc@engineering.ucsb.edu

Present Addresses
[‡]Institut für Chemie, Technische Universität Berlin, Sekretariat C 2, Straße des 17. Juni 135, 10623 Berlin, Germany.
[§]CEMHTI CNRS UPR3079, Université d'Orléans, 1D, avenue de la recherche-scientifique, 45071 Orléans Cedex 2, France.

ACKNOWLEDGMENT

The authors thank Dr. T. Zawodzinski, Dr. S. L. Scott, and Dr. K. D. Kreuer for helpful discussions. This work was supported in part by USARO through the Institute for Collaborative Biotechnologies at UCSB (Contract No. W911NF-09-D-0001) and through the MURI program (Grant No. DAAD 19-03-1-0121), by AmberWave, Inc., and by the Grand Technion Energy Program (GTEP) and Leona & Harry B. Helmsley Charitable Trust. D.K. acknowledges the Institute for Multiscale Materials Studies at Los Alamos National Laboratory (UC Santa Barbara Contract No. 113144) for a research stipend. Characterization measurements made use of the Central Facilities of the UCSB Materials Research Laboratory supported by the MRSEC Program of the NSF under Award No. DMR 05-20415. The authors thank BASF for the donation of Pluronic F127 triblock copolymer. B.F.C. was a 2006 Joseph Meyerhoff Visiting Professor at the Weizmann Institute of Science, Rehovot, Israel. DFT calculations were conducted using resources and services provided by the CRIHAN computing center (Haute Normandie, France, http://www.crihan.fr) under allocation No. 2009008.

REFERENCES

(1) Alvarez, F.; Ribeiro, F. R.; Perot, G.; Thomazeau, C.; Guisnet, M. *J. Catal.* **1996**, *162*, 179.
(2) Girgis, M. J.; Tsao, Y. P. *Ind. Eng. Chem. Res.* **1996**, *35*, 386.
(3) Adams, R. D.; Captain, B. *J. Organomet. Chem.* **2004**, *689*, 4521.
(4) Alexeev, O. S.; Gates, B. C. *Ind. Eng. Chem. Res.* **2003**, *42*, 1571.
(5) Marković, N. M.; Schmidt, T. J.; Stamenković, V.; Ross, P. N. *Fuel Cells* **2001**, *1*, 105.
(6) Sinfelt, J. H. *Bimetallic Catalysts: Discoveries, Concepts, And Applications*; Wiley: New York, 1983.
(7) Wasilke, J. C.; Obrey, S. J.; Baker, R. T.; Bazan, G. C. *Chem. Rev.* **2005**, *105*, 1001.
(8) Shylesh, S.; Wagener, A.; Seifert, A.; Ernst, S.; Thiel, W. R. *Angew. Chem., Int. Ed.* **2010**, *49*, 184.
(9) Davis, M. E.; Lobo, R. F. *Chem. Mater.* **1992**, *4*, 756.
(10) Wachs, I. E. *Catal. Today* **2005**, *100*, 79.
(11) *Transition Metal Oxides: Surface Chemistry and Catalysis*; Kung, H. H., Eds.; Studies in Surface Science and Catalysis, Vol. 45; Elsevier: Amsterdam, 1989.
(12) Zeidan, R. K.; Hwang, S. J.; Davis, M. E. *Angew. Chem., Int. Ed.* **2006**, *45*, 6332.
(13) Asefa, T.; Kruk, M.; MacLachlan, M. J.; Coombs, N.; Grondey, H.; Jaroniec, M.; Ozin, G. A. *J. Am. Chem. Soc.* **2001**, *123*, 8520.
(14) Margolese, D.; Melero, J. A.; Christiansen, S. C.; Chmelka, B. F.; Stucky, G. D. *Chem. Mater.* **2000**, *12*, 2448.
(15) Macquarrie, D. J.; Jackson, D. B.; Tailland, S.; Wilson, K.; Clark, J. H. In *Nanoporous Materials II*; Sayari, A.; Jaroniec, M.; Pinnavaia, T. J., Eds.; Studies in Surface Science and Catalysis, Vol. 129; Elsevier: Amsterdam, 2000; pp 275−282.
(16) Hall, S. R.; Fowler, C. E.; Lebeau, B.; Mann, S. *Chem. Commun.* **1999**, 201.
(17) Angelomé, P. C.; Soler-Illia, G. J. A. A. *J. Mater. Chem.* **2005**, *15*, 3903.
(18) Tanaka, S.; Kaihara, J.; Nishiyama, N.; Oku, Y.; Egashira, Y.; Ueyama, K. *Langmuir* **2004**, *20*, 3780.
(19) Petkov, N.; Mintova, S.; Jean, B.; Metzger, T.; Bein, T. *Mater. Sci. Eng., C* **2003**, *23*, 827.
(20) Che, S.; Liu, Z.; Ohsuna, T.; Sakamoto, K.; Terasaki, O.; Tatsumi, T. *Nature* **2004**, *429*, 281.
(21) Rodman, D. L.; Pan, H. J.; Clavier, C. W.; Feng, X. B.; Xue, Z. L. *Anal. Chem.* **2005**, *77*, 3231.
(22) Chen, C.; Yang, S. T.; Ahn, W. S.; Ryoo, R. *Chem. Commun* **2009**, 3627.
(23) Hoffmann, F.; Cornelius, M.; Morell, J.; Fröba, M. *Angew. Chem., Int. Ed.* **2006**, *45*, 3216.
(24) Soler-Illia, G. J. A. A.; Innocenzi, P. *Chem.—Eur. J.* **2006**, *12*, 4478.
(25) Sayari, A.; Hamoudi, S. *Chem. Mater.* **2001**, *13*, 3151.
(26) Stein, A.; Melde, B. J.; Schroden, R. C. *Adv. Mater.* **2000**, *12*, 1403.
(27) Yang, Q. H.; Liu, J.; Zhang, L.; Li, C. *J. Mater. Chem.* **2009**, *19*, 1945.
(28) Melero, J. A.; van Grieken, R.; Morales, G. *Chem. Rev.* **2006**, *106*, 3790.
(29) Wight, A. P.; Davis, M. E. *Chem. Rev.* **2002**, *102*, 3589.
(30) Burkett, S. L.; Sims, S. D.; Mann, S. *Chem. Commun.* **1996**, 1367.
(31) Macquarrie, D. J. *Chem. Commun.* **1996**, 1961.
(32) Lim, M. H.; Blanford, C. F.; Stein, A. *J. Am. Chem. Soc.* **1997**, *119*, 4090.
(33) Müller, C. A.; Schneider, M.; Mallat, T.; Baiker, A. *Appl. Catal., A* **2000**, *201*, 253.
(34) Mercier, L.; Pinnavaia, T. J. *Environ. Sci. Technol.* **1998**, *32*, 2749.
(35) Molenkamp, W. C.; Watanabe, M.; Miyata, H.; Tolbert, S. H. *J. Am. Chem. Soc.* **2004**, *126*, 4476.
(36) Angeomé, P. C.; Soler-Illia, G. J. A. A. *Chem. Mater.* **2005**, *17*, 322.
(37) Asefa, T.; MacLachlan, M. J.; Coombs, N.; Ozin, G. A. *Nature* **1999**, *402*, 867.
(38) Díaz, I.; Márquez-Alvarez, C.; Mohino, F.; Pérez-Pariente, J.; Sastre, E. *J. Catal.* **2000**, *193*, 283.
(39) Fowler, C. E.; Lebeau, B.; Mann, S. *Chem. Commun.* **1998**, 1825.
(40) Alvaro, M.; Corma, A.; Das, D.; Fornés, V.; García, H. *J. Catal.* **2005**, *231*, 48.
(41) Dufaud, V.; Davis, M. E. *J. Am. Chem. Soc.* **2003**, *125*, 9403.
(42) Moller, K.; Bein, T. *Chem. Mater.* **1998**, *10*, 2950.
(43) Bernardos, A.; Aznar, E.; Marcos, M. D.; Martínez-Máñez, R.; Sancenón, F.; Soto, J.; Barat, J. M.; Amorós, P. *Angew. Chem., Int. Ed.* **2009**, *48*, 5884.
(44) Athens, G. L.; Ein-Eli, Y.; Chmelka, B. F. *Adv. Mater.* **2007**, *19*, 2580.
(45) Zhang, J. L.; Xie, Z.; Zhang, J. J.; Tang, Y. H.; Song, C. J.; Navessin, T.; Shi, Z. Q.; Song, D. T.; Wang, H. J.; Wilkinson, D. P.; Liu, Z. S.; Holdcroft, S. *J. Power Sources* **2006**, *160*, 872.
(46) Kreuer, K. D. *J. Membr. Sci.* **2001**, *185*, 29.
(47) Jannasch, P. *Curr. Opin. Colloid Interface Sci.* **2003**, *8*, 96.
(48) Li, Q. F.; He, R. H.; Jensen, J. O.; Bjerrum, N. J. *Chem. Mater.* **2003**, *15*, 4896.
(49) Wang, H. T.; Holmberg, B. A.; Huang, L. M.; Wang, Z. B.; Mitra, A.; Norbeck, J. M.; Yan, Y. S. *J. Mater. Chem.* **2002**, *12*, 834.
(50) Chen, Z. W.; Holmberg, B.; Li, W. Z.; Wang, X.; Deng, W. Q.; Munoz, R.; Yan, Y. S. *Chem. Mater.* **2006**, *18*, 5669.
(51) Holmberg, B. A.; Wang, X.; Yan, Y. S. *J. Membr. Sci.* **2008**, *320*, 86.
(52) So, S. Y.; Kim, S. C.; Lee, S. Y. *J. Membr. Sci.* **2010**, *360*, 210.
(53) Di Vona, M. L.; Sgreccia, E.; Donnadio, A.; Casciola, M.; Chailan, J. F.; Auer, G.; Knauth, P. *J. Membr. Sci.* **2011**, *369*, 536.
(54) Moghaddam, S.; Pengwang, E.; Jiang, Y.-B.; Garcia, A. R.; Burnett, D. J.; Brinker, C. J.; Masel, R. I.; Shannon, M. A. *Nat. Nanotechnol.* **2010**, *5*, 230.
(55) Zhao, D.; Yang, P.; Melosh, N.; Feng, J.; Chmelka, B. F.; Stucky, G. D. *Adv. Mater.* **1998**, *10*, 1380.
(56) Luan, Z. H.; Hartmann, M.; Zhao, D. Y.; Zhou, W. Z.; Kevan, L. *Chem. Mater.* **1999**, *11*, 1621.
(57) Vega, A. J. *J. Am. Chem. Soc.* **1988**, *110*, 1049.
(58) (a) Janicke, M. T.; Landry, C. C.; Christiansen, S. C.; Kumar, D.; Stucky, G. D.; Chmelka, B. F. *J. Am. Chem. Soc.* **1998**, *120*, 6940. (b) Hayashi, S.; Hayamizu, K. *Bull. Chem. Soc. Jpn.* **1991**, *64*, 685. (c) Dargaville, T. R.; George, G. A; Hill, D. J. T.; Scheler, U.; Whittaker, A. K. *Macromolecules* **2002**, *35*, 5544.
(59) Chmelka, B. F.; Zwanziger, J. W. Solid-State NMR Line Narrowing Methods for Quadrupolar Nuclei: Double Rotation and Dynamic-Angle Spinning. In *NMR Basic Principles and Progress*; Kosfeld, P., Blümich, B., Eds.; Springer-Verlag: Berlin, 1997; pp 79−124.
(60) Bourgeat-Lami, E.; Massiani, P.; Di Renzo, F.; Espiau, P.; Fajula, F. *Appl. Catal.* **1991**, *72*, 139.
(61) Frisch, M. J. et al. *Gaussian 03*, Revision C.02; Gaussian, Inc.: Wallingford, CT, 2004.
(62) Becke, A. D. *J. Chem. Phys.* **1993**, *98*, 5648.
(63) Lee, C. T.; Yang, W. T.; Parr, R. G. *Phys. Rev. B* **1988**, *37*, 785.
(64) Ditchfield, R. *Mol. Phys.* **1974**, *27*, 789.
(65) Ziegler, T. *Chem. Rev.* **1991**, *91*, 651.
(66) Feller, D. *J. Comput. Chem.* **1996**, *17*, 1571.
(67) Schuchardt, K. L.; Didier, B. T.; Elsethagen, T.; Sun, L. S.; Gurumoorthi, V.; Chase, J.; Li, J.; Windus, T. L. *J. Chem. Inf. Model.* **2007**, *47*, 1045.
(68) Hedin, N.; Graf, R.; Christiansen, S. C.; Gervais, C.; Hayward, R. C.; Eckert, J.; Chmelka, B. F. *J. Am. Chem. Soc.* **2004**, *126*, 9425.
(69) Zhao, D. Y.; Yang, P. D.; Margolese, D. I.; Chmelka, B. F.; Stucky, G. D. *Chem. Commun.* **1998**, 2499.
(70) Janicke, M. T.; Landry, C. C.; Christiansen, S. C.; Birtalan, S.; Stucky, G. D.; Chmelka, B. F. *Chem. Mater.* **1999**, *11*, 1342.
(71) The transformation of framework aluminosilica species on the mesochannel surfaces from Al^{IV} moieties before incorporating perfluorinated-sulfonic-acid grafting species into predominantly Al^{VI}

species afterward is not expected to involve significant dissolution and redeposition of aluminosilica moieties under the conditions used.

(72) Engelhardt, G.; Michel, D. *High-Resolution Solid-State NMR of Silicates and Zeolites*; Wiley & Sons: New York, 1987; p 114.

(73) Gerstein, B. C. *Philos. Trans. R. Soc. London, Ser. A* **1981**, *299*, 521.

(74) The broad weak intensity in the region 0 to −40 ppm in the 1D ^{27}Al MAS spectrum of Figure 2b could be due to a distribution of the principal component V_{zz} of the $^{27}Al^{VI}$ electric-field-gradient tensor or to a separate broad signal. Czjzek-type analyses of ^{27}Al signals in disordered solids yield skewed low-frequency intensity consistent with a distribution of V_{zz} values, although the measured ^{27}Al intensity distribution differs from several Czjzek-type lineshapes that have been reported.[75,76] The 2D ^{27}Al{^{1}H} HETCOR spectrum (Figure 2b) shows that the low-frequency ^{27}Al intensity is correlated to a distribution of ^{1}H signals associated with adsorbed water molecules.

(75) de Lacaillerie, J. B. D.; Fretigny, C.; Massiot, D. *J. Magn. Reson.* **2008**, *192*, 244.

(76) Le Caër, G.; Bureau, B.; Massiot, D. *J. Phys.: Condens. Matter* **2010**, *22*, 065402.

(77) Montanari, L.; de Angelis, A.; Carati, C. *Appl. Magn. Reson.* **1997**, *12*, 329.

(78) Simpler grafted moieties, such as $-OCF_2CH_3$, with fewer degrees of freedom were additionally considered and yielded similar results.

(79) Murthi, V. S.; Urian, R. C.; Mukerjee, S. *J. Phys. Chem. B* **2004**, *108*, 11011.

(80) Chin, D. T.; Chang, H. H. *J. Appl. Electrochem.* **1989**, *19*, 95.

(81) Casciola, M.; Alberti, G.; Sganappa, M.; Narducci, R. *J. Power Sources* **2006**, *162*, 141.

(82) Halseid, R.; Vie, P. J. S.; Tunold, R *J. Electrochem. Soc.* **2004**, *151*, A381.

(83) Park, Y. S.; Hatae, T.; Itoh, H.; Jang, M. Y.; Yamazaki, Y. *Electrochim. Acta* **2004**, *50*, 595.

(84) Blumenthal, G.; Cappadonia, M.; Lehmann, M. *Ionics* **1996**, *2*, 102.

(85) Sone, Y.; Ekdunge, P.; Simonsson, D. *J. Electrochem. Soc.* **1996**, *143*, 1254.

(86) Alberti, G.; Casciola, M; Massinelli, L; Bauer, B. *J. Membr. Sci.* **2001**, *185*, 73.

(87) Apparent activation energies associated with proton transport and viscosity effects in bulk aqueous solutions of trifluoromethanesulfonic acid (λ = 1) were estimated from temperature-dependent proton conductivity data,[88] using a linearized Arrhenius equation.

(88) Barthel, J; Meier, R.; Conway, B. E. *J. Chem. Eng. Data* **1999**, *44*, 155.

(89) Zawodzinski, T. A.; Springer, T. E.; Davey, J.; Jestel, R.; Lopez, C.; Valerio, J.; Gottesfeld, S. *J. Electrochem. Soc.* **1993**, *140*, 1981.

(90) Kopitzke, R. W.; Linkous, C. A.; Anderson, H. R.; Nelson, G. L. *J. Electrochem. Soc.* **2000**, *147*, 1677.

SUPPORTING INFORMATION

Molecular Optimization of Multiply-Functionalized Mesoporous Films with Ion Conduction Properties

*George L. Athens,[1] Donghun Kim,[1] Jan D. Epping,[1] Sylvian Cadars,[1] Yair Ein-Eli,[2] Bradley F. Chmelka[1]**

[1] *Department of Chemical Engineering, University of California, Santa Barbara, California 93106 USA*

[2] *Department of Materials Engineering, Technion, 32000, Haifa, Israel*

*Corresponding author: bradc@engineering.ucsb.edu

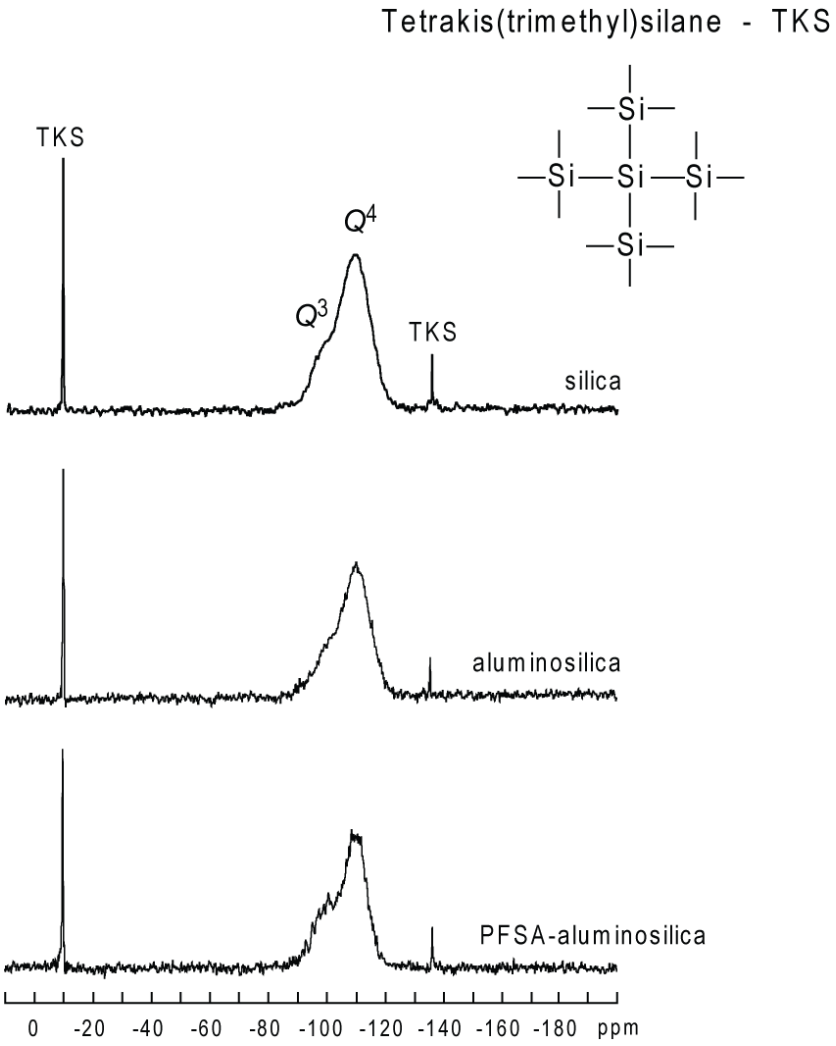

Supplemental Figure S1. Quantitative single-pulse ^{29}Si MAS NMR spectra acquired for a cubic mesoporous silica film, following surface-grafting of the same mesoporous silica film with aluminosilica (3.5 wt% Al), and following additional surface-grafting with perfluorinated sulfonic acid species (5 wt% PFSA, 3.5 wt% Al). All spectra were quantified using 2 mg tetrakis(trimethyl)silane (TKS) as an internal spin-counting standard.

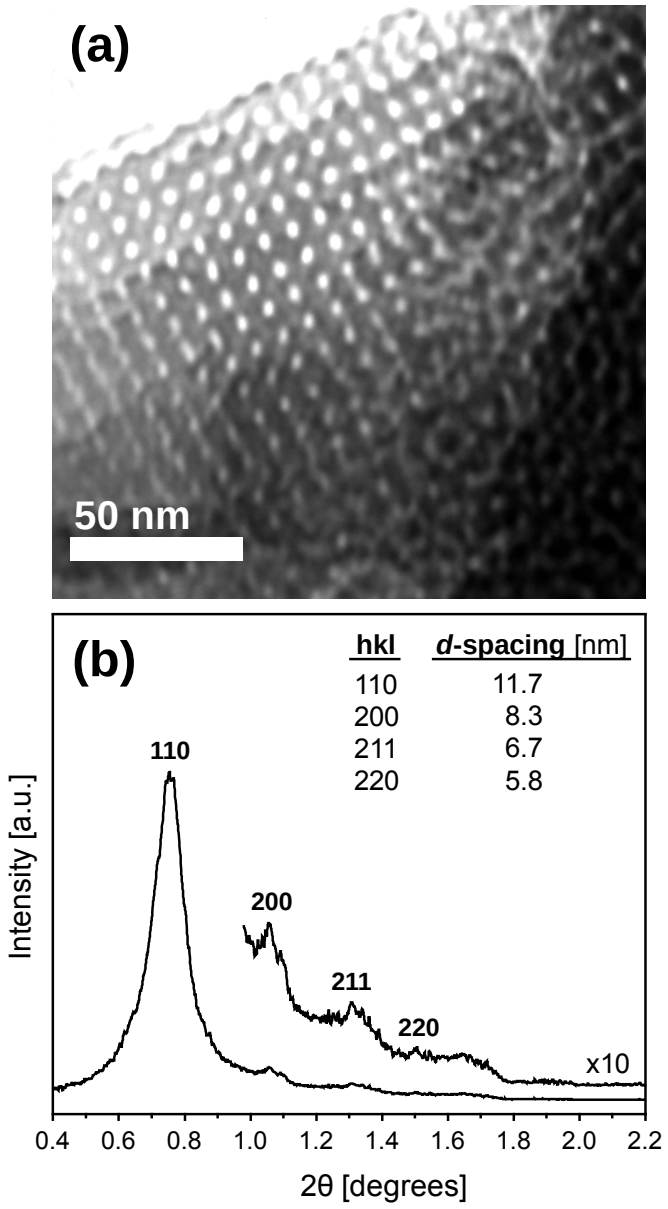

Supplemental Figure S2. (a) Transmission electron microscopy image and (**b)** small-angle X-ray scattering pattern for perfluorosulfonic-acid-grafted cubic mesoporous aluminosilica (5 wt% PFSA, 3.5 wt% Al) film. The diffraction pattern is indexed to the body-centered-cubic ($Im\bar{3}m$) structure. The 1D plot is the azimuthal integral of a 2D scattering pattern obtained by transmission-mode XRD with the beam oriented perpendicular to the plane of the films.

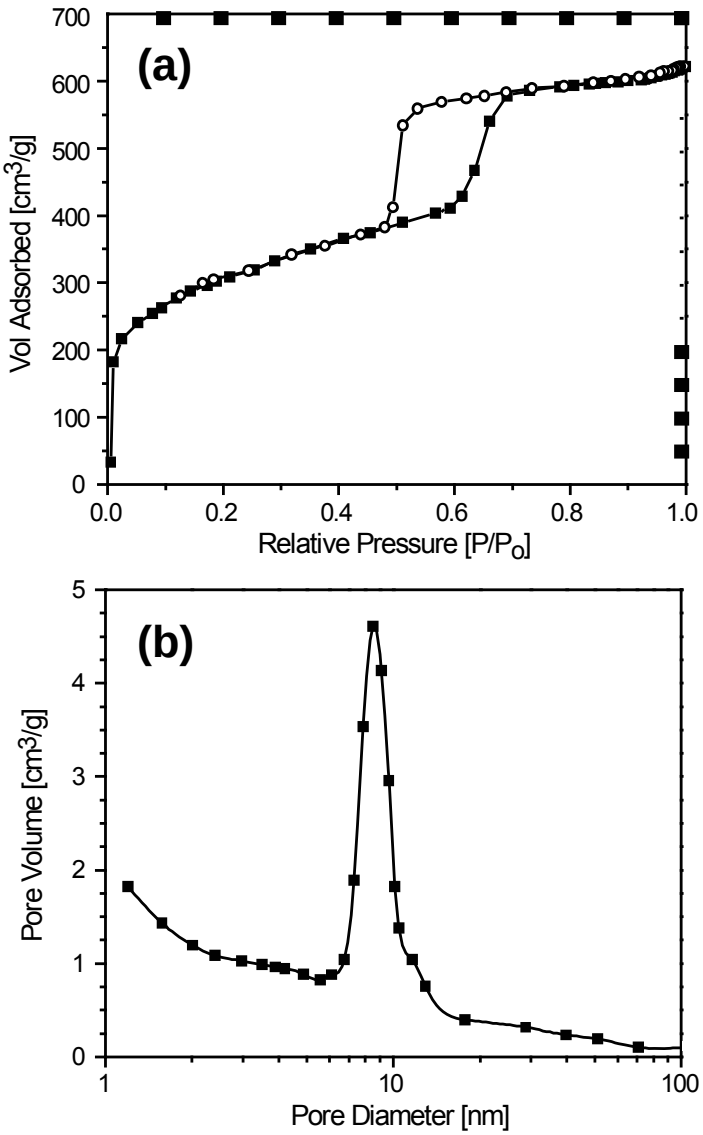

Supplemental Figure S3. (a) Nitrogen adsorption [■] - desorption [○] isotherms acquired at 77 K and (**b)** mesopore-size-distribution plot obtained from a Barrett-Joyner-Halenda (BJH) analysis of the adsorption isotherm branch for the perfluorosulfonic-acid-grafted cubic mesoporous aluminosilica (5 wt% PFSA, 3.5 wt% Al) film material with body-centered-cubic ($Im\bar{3}m$) ordering (no triflic acid).

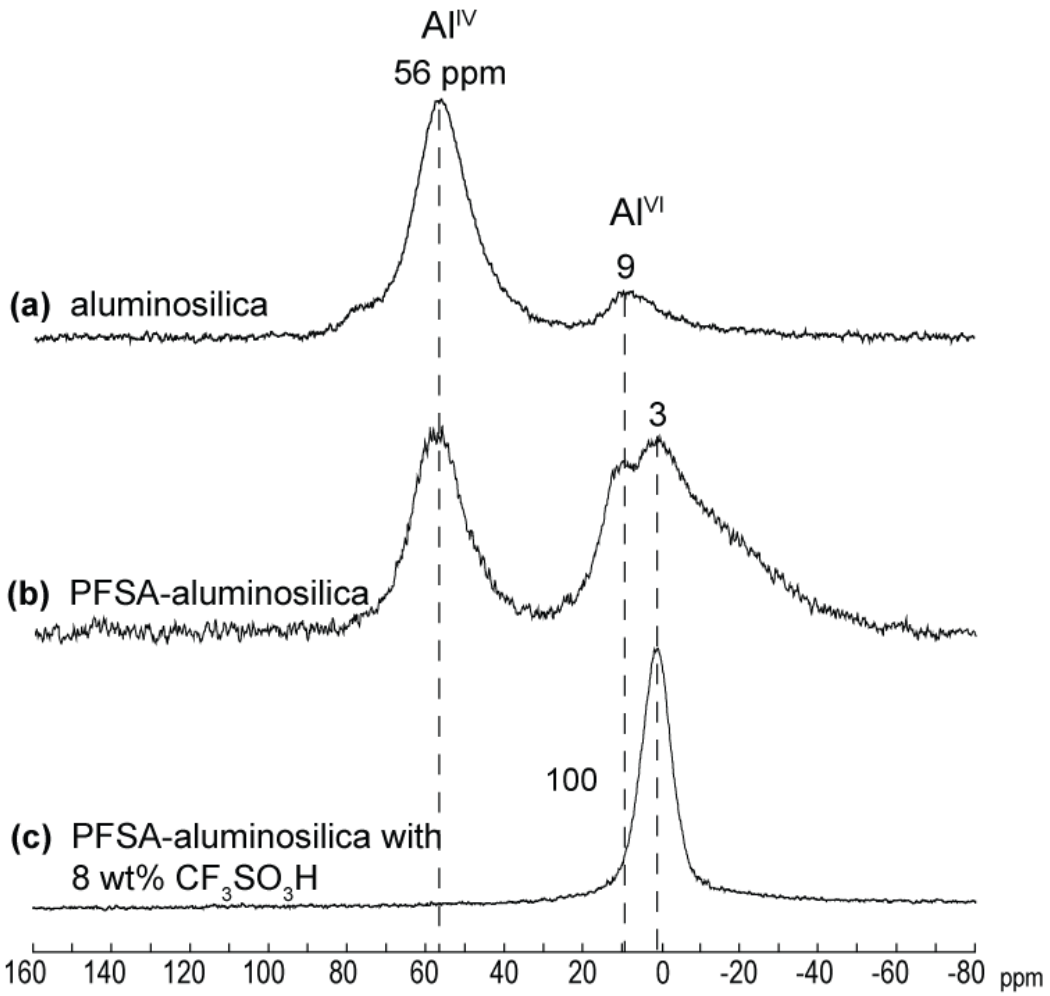

Supplemental Figure S4. Solid-state 1D single-pulse ^{27}Al MAS NMR spectra of **(a)** cubic mesoporous aluminosilica (3.7 wt% Al), **(b)** cubic mesoporous PFSA-grafted aluminosilica (5 wt% PFSA, 3.5 wt% Al), and **(c)** cubic PFSA-grafted mesoporous aluminosilica (5 wt% PFSA, 3.5 wt% Al) containing 8 wt% CF_3SO_3H acid backfilled into the mesopores. The relative integrated signal intensities in the spectra correspond to the relative populations of the different four- and six-coordinate ^{27}Al species shown in Table 1. Absolute quantification of the signals was achieved by comparison with the integrated ^{27}Al intensity at 113 ppm from a 2-mg piece of ^{27}AlN used as a secondary spin-counting standard (spectra not shown here).

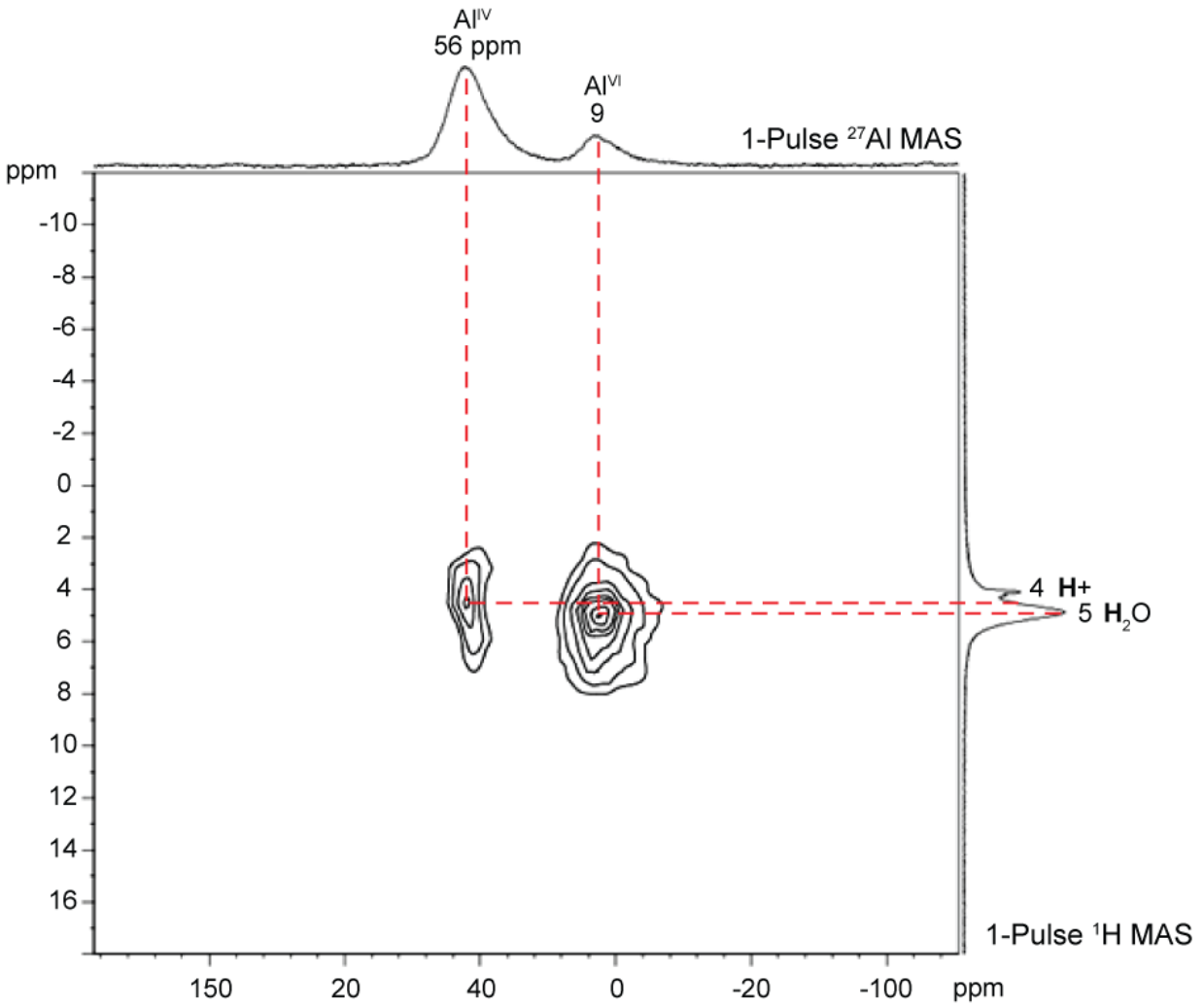

Supplemental Figure S5. Solid-state 2D ^{27}Al{^{1}H} HETCOR spectrum at room temperature for the cubic mesoporous aluminosilica (3.7 wt% Al) without grafted PFSA or adsorbed triflic acid (same sample as Fig. S4a). Separate 1D single-pulse ^{27}Al and ^{1}H MAS spectra are plotted along their corresponding axes.

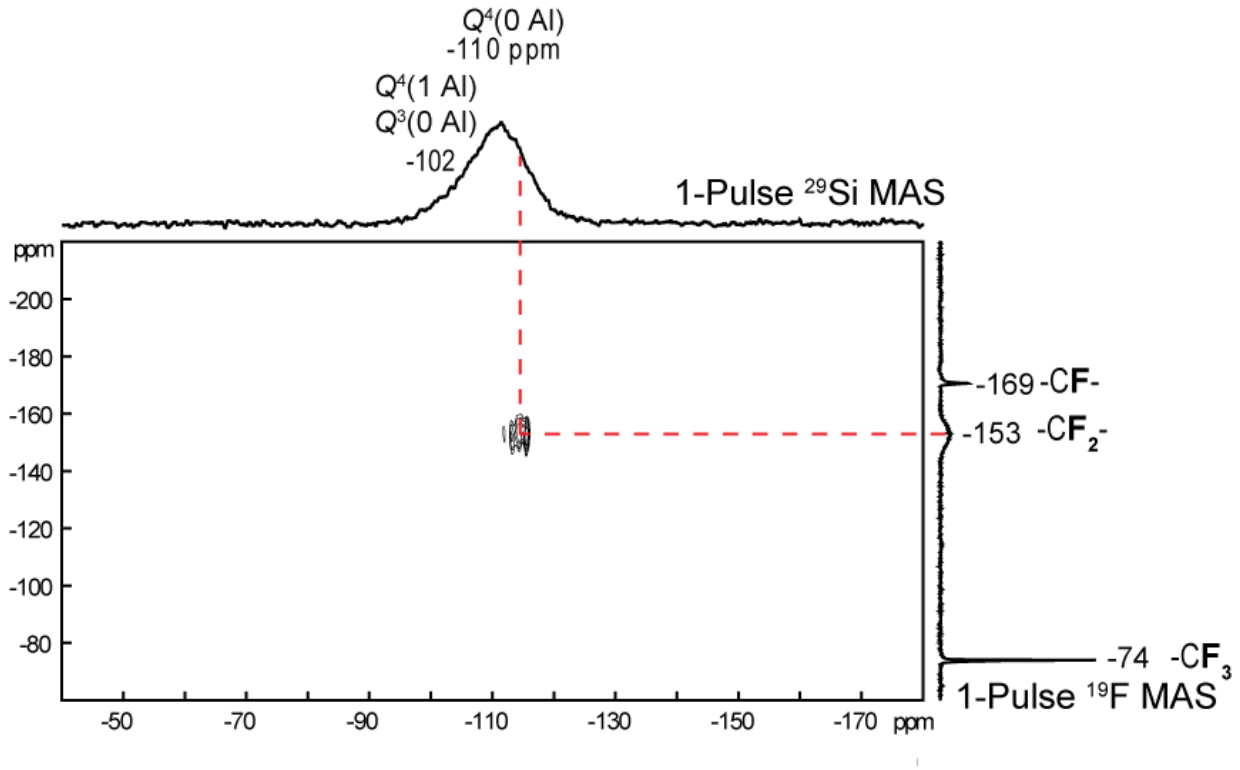

Supplemental Figure S6. Solid-state 2D $^{29}Si\{^{19}F\}$ HETCOR spectrum acquired at room temperature for the cubic mesoporous perfluorosulfonic-acid-grafted aluminosilica (5 wt% PFSA, 3.5 wt% Al) prior to backfilling of the mesopores with triflic acid. Separate 1D single-pulse ^{29}Si and ^{19}F MAS spectra are plotted along their corresponding axes. The 2D HETCOR contour plot shows correlated signal intensity between the $–CF_2–$ ^{19}F atoms of the grafted PFSA and surface Q^3 ^{29}Si moieties near the silica grafting site (see text).

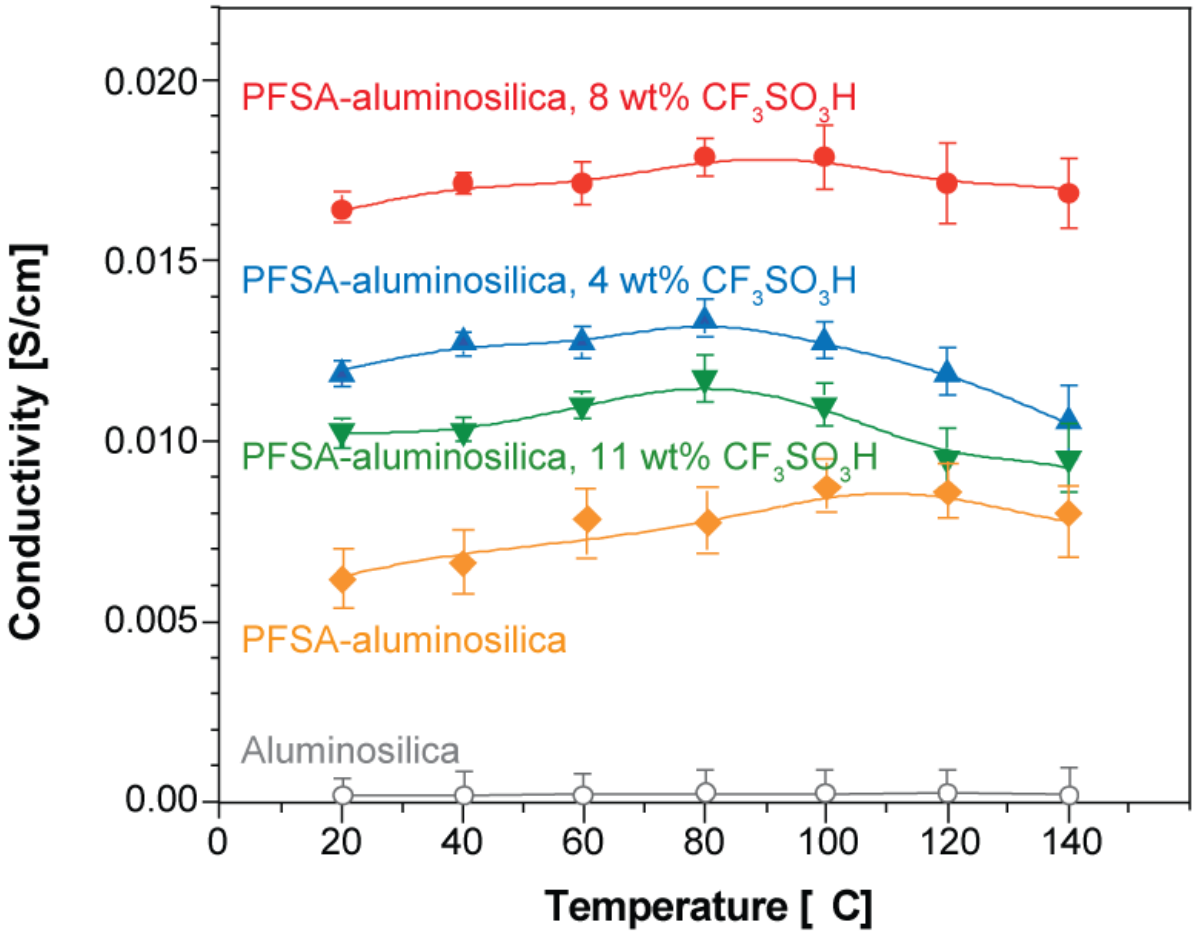

Supplemental Figure S7. Proton conductivity as a function of temperature at 50% RH for otherwise identical 65-µm-thick 5 wt% PFSA- and 3.5 wt% Al aluminosilica-grafted cubic mesoporous silica films containing different amounts of mesopore-filling triflic acid: [♦] 0 wt%, [▲] 4 wt%, [●] 8 wt%, and [▼] 11 wt% CF_3SO_3H acid. The conductivity of cubic mesoporous aluminosilica (3.7 wt% Al) without co-grafted-PFSA or triflic acid species is shown for comparison [○]. The effects of the different aluminosilica, perfluorosulfonic acid, and triflic acid optimization criteria identified and discussed in the text can be clearly seen, where the macroscopic proton conductivities of differently functionalized films are plotted as functions of temperature. A cubic mesoporous silica film grafted with aluminosilica (3.7 wt% Al) and no perfluorosulfonic acid species (grey) displays negligible proton conductivity. By comparison, a

PFSA-grafted aluminosilica film (5 wt% PFSA, 3.5 wt% Al) with no triflic acid back-filling the mesopores (yellow) exhibits stable proton conductivity values of $6–8\times10^{-3}$ S/cm between 20–180 °C. The introduction of 4 wt% triflic acid into the mesopores of an otherwise identical PFSA-grafted aluminosilica film (blue) increases the total acid concentration, leading to two-fold higher proton conductivity in this film, with a maximum value of 1.3×10^{-2} S/cm at 80-100 °C. This trend of increased triflic acid concentrations in the mesopores leading to higher proton conductivities in otherwise identical PFSA-functionalized cubic mesoporous aluminosilica films continues up to triflic acid loadings of 8 wt% (red). Over the temperature range 20-140 °C, high and stable proton conductivity values (up to 1.8×10^{-2} S/cm) were measured for a PFSA-grafted aluminosilica film containing 8 wt% triflic acid filling the mesopores. At still higher triflic acid loadings (e.g., 11 wt%), lower proton conductivities resulted (green).

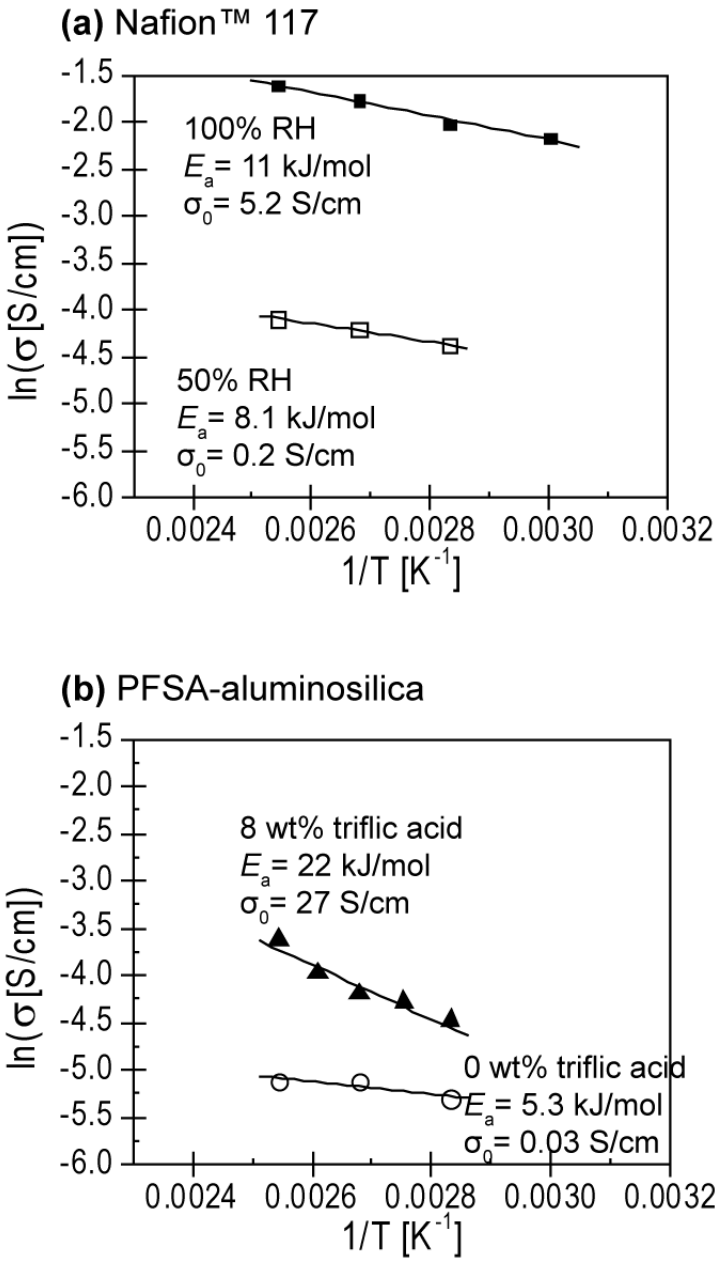

Supplemental Figure S8. Arrhenius plots of proton conductivities for **(a)** Nafion™ 117 at 100% [■] and 50% relative humidity (R.H.) [□] and **(b)** PFSA-aluminosilica functionalized membranes without [○] and with 8 wt% triflic acid [▲] at 50% R.H. The apparent activation energy (E_a) values shown are extracted from the slopes of the respective plots and pre-exponential factors from the *y*-intercepts. The conductivity values shown are consistent with those in Figure 6 of the manuscript.

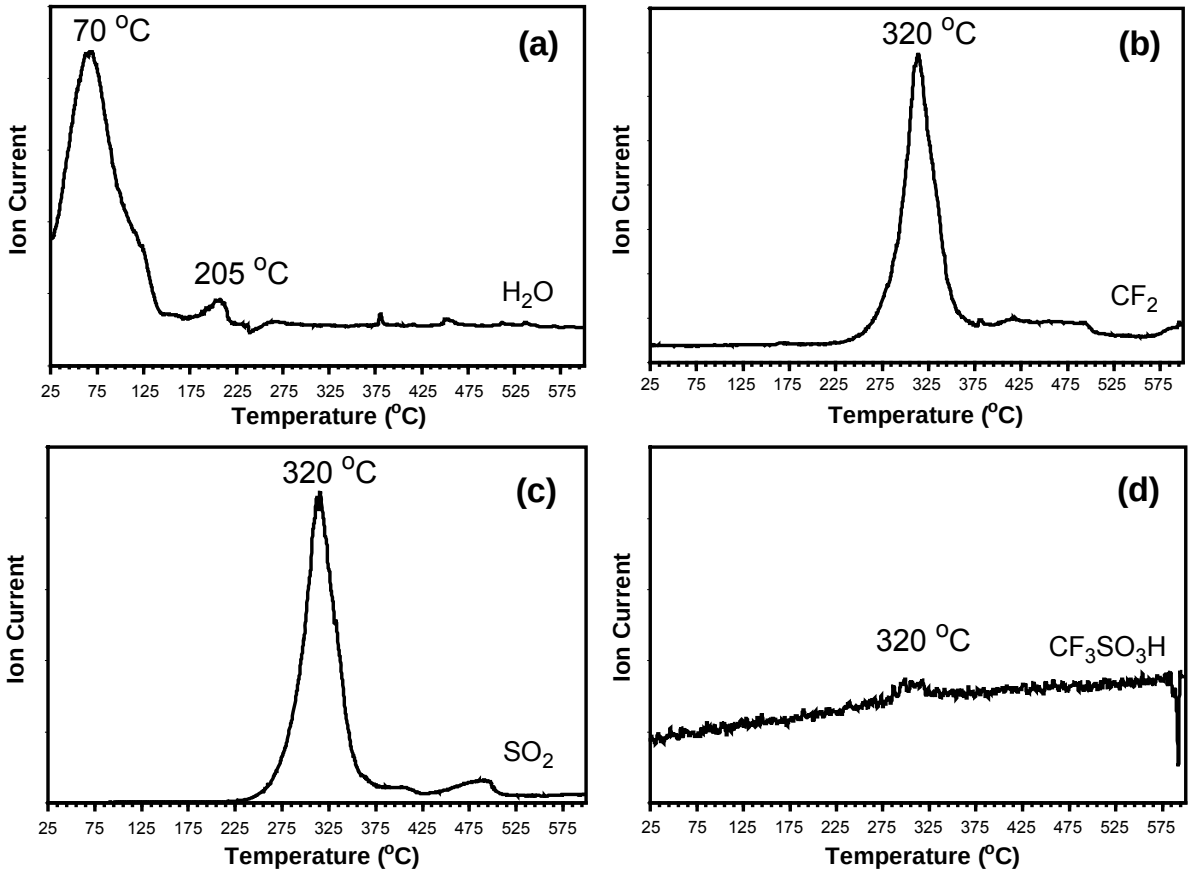

Supplemental Figure S9. Mass spectrometry measurements conducted simultaneously on the effluent gases from PFSA-grafted cubic mesoporous aluminosilica (5 wt% PFSA, 3.5 wt% Al) film containing 8 wt% triflic acid in the mesopores, as it was heated during thermogravimetric analysis. The ion currents measured are selective to species with specific molecular masses, such as **(a)** H_2O, **(b)** CF_2, **(c)** SO_2, and **(d)** CF_3SO_3H.

Complete reference 61:

Frisch, M. J.; Trucks, G. W.; Schlegel, H. B.; Scuseria, G. E.; Robb, M. A.; Cheeseman, J. R.; Montgomery, Jr., J. A.; Vreven, T.; Kudin, K. N.; Burant, J. C.; Millam, J. M.; Iyengar, S. S.; Tomasi, J.; Barone, V.; Mennucci, B.; Cossi, M.; Scalmani, G.; Rega, N.; Petersson, G. A.; Nakatsuji, H.; Hada, M.; Ehara, M.; Toyota, K.; Fukuda, R.; Hasegawa, J.; Ishida, M.; Nakajima, T.; Honda, Y.; Kitao, O.; Nakai, H.; Klene, M.; Li, X.; Knox, J. E.; Hratchian, H. P.; Cross, J. B.; Bakken, V.; Adamo, C.; Jaramillo, J.; Gomperts, R.; Stratmann, R. E.; Yazyev, O.; Austin, A. J.; Cammi, R.; Pomelli, C.; Ochterski, J. W.; Ayala, P. Y.; Morokuma, K.; Voth, G. A.; Salvador, P.; Dannenberg, J. J.; Zakrzewski, V. G.; Dapprich, S.; Daniels, A. D.; Strain, M. C.; Farkas, O.; Malick, D. K.; Rabuck, A. D.; Raghavachari, K.; Foresman, J. B.; Ortiz, J. V.; Cui, Q.; Baboul, A. G.; Clifford, S.; Cioslowski, J.; Stefanov, B. B.; Liu, G.; Liashenko, A.; Piskorz, P.; Komaromi, I.; Martin, R. L.; Fox, D. J.; Keith, T.; Al-Laham, M. A.; Peng, C. Y.; Nanayakkara, A.; Challacombe, M.; Gill, P. M. W.; Johnson, B.; Chen, W.; Wong, M. W.; Gonzalez, C.; Pople, J. A. *Gaussian 03, Revision C.02*, Gaussian, Inc.: Wallingford CT, 2004.